Geothermics 92 (2021) 102035

Contents lists available at ScienceDirect

Geothermics

journal homepage: www.elsevier.com/locate/geothermics

Extrapolation of populations of small earthquakes to predict consequences of low- probability high impact events: The Pohang case study revisited

Rob Westaway

James Watt School of Engineering, University of Glasgow, James Watt (South) Building, Glasgow, G12 8QQ, UK

ARTICLE INFO

Keywords:
Pohang
Korea
EGS
Earthquake
Seismicity
Risk

ABSTRACT

The magnitude (M_W) 5.5 Pohang, Korea, earthquake on 15 November 2017, induced by the Pohang Engineered Geothermal Systems (EGS) project, caused one fatality and ~US$300 million of economic consequences. The Commission, appointed by the Korean Government to investigate this earthquake, has made public a release of data including magnitudes of the smaller earthquakes associated with the well stimulations. On the basis of this earthquake population, it has been proposed that a significant probability of such losses was predictable beforehand, and that the project should have been suspended, implying that its developer was remiss for not doing so. This argument depends on the low b-value estimated, ~0.61. However, three factors are shown to contribute, individually or in combination, to inaccuracy of these magnitude determinations: the low recording bandwidth of the permanent seismograph stations in the area; miscalibration of the formula for determining local magnitudes in Korea; and the relation used to estimate magnitudes of smaller events from larger events by template matching. These factors all cause underestimation of magnitudes of the smallest events documented, resulting in underestimation of b-values. The true b-values are higher, being 1.12 for the earthquakes associated with the August 2017 stimulation of well PX-1; similar values are estimated for the other well stimulations. A consequence of this analysis is that the probability of any earthquake as large as $M_W = 5.5$, predicted ahead of its occurrence by extrapolation using b-values, was much lower than has been claimed. This analysis highlights the need for agreed workflow specifications for reporting datasets like this, where the data might influence prosecution of EGS developers, as well as agreed specifications for acceptable economic risk arising from EGS projects.

1. Introduction

The EGS project near the Korean city of Pohang (Fig. 1) has been thoroughly described (e.g., Lee et al., 2011; Yoon et al., 2015; Grigoli et al., 2018; Kim Kwang-Hee et al., 2018; Kim Kwang-Il et al., 2018; Ellsworth et al., 2019; Hofmann et al., 2019; Lee et al., 2019; GSK, 2019). In summary (Fig. 2), well PX-1 was initially drilled vertically into the Permian Pohang granite, then side-tracked to a point ~600 m WNW at ~4.2 km depth. Vertical well PX-2 reaches a similar depth; in November 2015, during its drilling, mud loss, accompanied by small earthquakes, occurred into what proved to be the seismogenic fault, named the Namsong Fault, of the 15 November 2017 $M_W = 5.5$ earthquake. However, this 2015 seismicity, which indicated that this fault was critically stressed, went unreported at the time; it was recognized later (Kim Kwang-Hee et al., 2018) when archived data from seismograph station PHA2, ~10 km north of the site, were examined. PHA2 is part of a network of permanent stations operated by the Korea Meteorological Administration (KMA) to monitor regional seismicity (Fig. 3(a)); the temporary seismograph network around the EGS site (Fig. 3(b)) was not yet operational. Five stimulations took place to try to create a hydraulic connection through the granite between the wells: in PX-2 in February 2016, April 2017, and September 2017; and in PX-1 in December 2016 and August 2017. This EGS project was implemented by Korean organizations led by the Pohang Geothermal Power Co., a subsidiary of NexGeo Inc. (www.nexgeo.com), who were responsible for all activities.

The 15 November 2017 $M_W = 5.5$ earthquake caused one fatality and ~US$300 million of economic consequences, making it by far the largest associated with any EGS project. The Korean government appointed a Commission to investigate whether this project caused the earthquake, NexGeo being thereby required to disclose project data. These data, plus other evidence including data from permanent seismograph stations (notably, station PHA2), informed the Commission reports (Lee et al., 2019; GSK, 2019); Commission members have also used this dataset in publications (e.g., Ellsworth et al., 2019; Woo et al., 2019; Langenbruch et al., 2020; Yeo et al., 2020), which include strong criticisms of the

E-mail address: robert.westaway@gla.ac.uk.

https://doi.org/10.1016/j.geothermics.2020.102035
Received 23 June 2020; Received in revised form 14 October 2020; Accepted 22 December 2020
Available online 17 February 2021

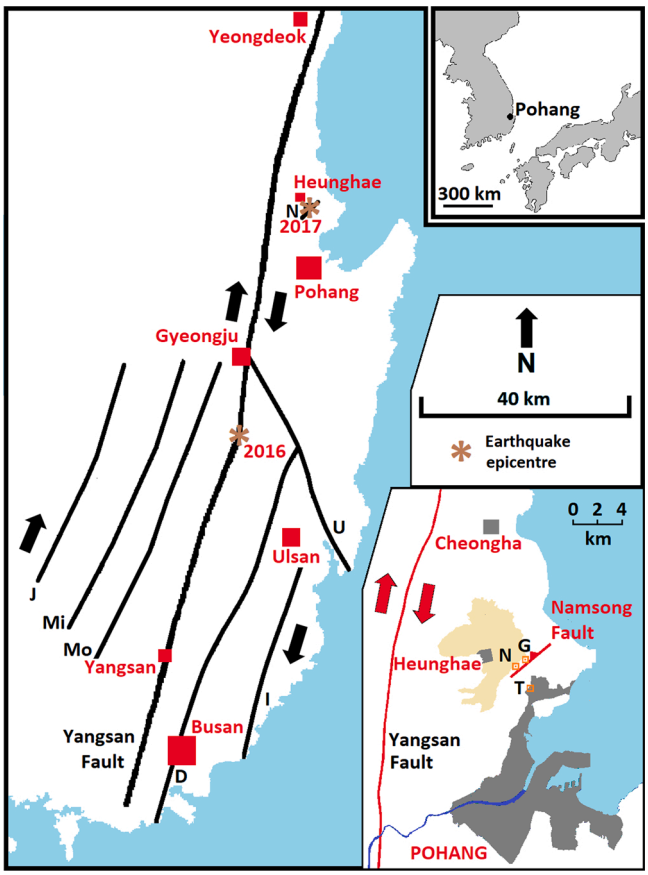

Fig. 1. Location map for the city of Pohang in the SE part of the Korean peninsula (upper inset showing wider location, lower inset showing greater local detail), showing Late Cenozoic right-lateral faults, the Namsong Fault, and the epicentres of the 12 September 2016 and 15 November 2017 earthquakes (both of $M_W \sim 5.5$). The local inset shows the Namsong Fault (depicted schematically), the Heunghae alluvial plain (pale shading), the EGS project site (G), Namsong village (N), and the Pohang thermal spa resort that yielded hydrochemical data (T). Modified from Fig. 1 of Westaway and Burnside (2019) .

management of the EGS project. In parallel, participants in the DESTRESS ('Demonstration of soft stimulation treatments of geothermal reservoirs') Horizon 2020 project have developed much of the current understanding of this earthquake, notably for aspects unexplored by the Commission (e.g., Grigoli et al., 2018; Westaway and Burnside, 2019; Westaway et al., 2020). It has been proposed that the $M_W = 5.5$ earthquake was caused by poroelastic changes to the state of stress on the Namsong Fault resulting from the well stimulations (e.g., Yeo et al., 2020). It has also been suggested that this earthquake resulted from the effect of injected surface water entering the fault and dissolving minerals, bringing it closer to the condition for slip (e.g., Westaway and Burnside, 2019; Westaway et al., 2020). Conceivably, both these mechanisms contributed, the unresolved issue being their relative importance to changing the state of stress; however, neither mechanism requires any causal connection with the numbers of small events during the stimulations. In parallel to these scientific activities, legal enquiries have proceeded into whether anyone responsible for this EGS project should face trial for manslaughter. These legal actions have been informed by the available data; their validity thus depends on the accuracy of these data.

Immediately after the GSK (2019) report was released, mismatch was noted between the magnitudes thus reported (using a variety of methods, as will be discussed below: some as moment magnitude M_W; some as local magnitude M_L; others as proxy magnitudes intended to equate to M_W and/or M_L) and those determined for the August 2017 stimulation of well PX-1, which was carried out as part of DESTRESS (Hofmann et al., 2019), the Hofmann et al. (2019) magnitudes (M_W) being significantly higher for events in common between the populations. The Hofmann et al. (2019) magnitudes were used to implement the 'traffic light scheme' for this stimulation; thus, if they were systematically in error, the stimulation was not implemented to its stated protocol. On the other hand, if the magnitudes reported by GSK (2019) were in error, then the associated low b-values determined for the earthquake populations might be incorrect and conclusions derived from them, regarding the high probability of occurrence of a large earthquake and of the associated casualties and damage, and the associated repeated criticisms of the EGS project management for not terminating the project beforehand (e.g., Ellsworth et al., 2019; Langenbruch et al., 2020), would be inappropriate. Either way, it is important to assess the possibility of systematic error affecting either set of magnitude determinations.

A great diversity of procedures exists for determining local magnitude (M_L) in different jurisdictions worldwide. In recent years multiple instances have emerged where the accuracy of such scales has been called into question, especially for smaller events. For example, Amato and Mele (2008) noted that M_L estimates for a given earthquake in Italy were significantly higher for nearby stations than for more distant stations, suggesting miscalibration of the distance-dependence in the formula used for M_L. A similar problem was noted for the formula used by the British Geological Survey (BGS) for determining M_L in the UK (e.g., Ottemöller and Sargeant, 2013; Butcher et al., 2017; Luckett et al., 2019) and was of particular significance because a regulatory threshold of M_L 0.5 had been specified for earthquakes caused by 'fracking'; the miscalibration meant that M_L values of such events, recorded only by nearby stations, would be exaggerated. A workaround has since been introduced to deal with this issue (Luckett et al., 2019). On the other hand, Uchide and Imanishi (2018) noted that M_L values routinely determined by seismograph networks for small earthquakes in Japan are systematically underestimated. These authors attributed this effect as a consequence of much of the seismic signal amplitude for these events being 'lost' because of the sparse digital sampling in operation, at only 100 samples per second. National network stations in Korea also sample 100 times a second (see below), and might be similarly affected. Kwiatek and Ben- Zion (2016) likewise noted that low sampling rates can affect the ability of networks to accurately determine earthquake source parameters, such as seismic moment M_O and thus M_W, and – by filtering out high frequencies – can also degrade the ability of networks to detect small events. These authors indeed remarked that failure to recognize these issues may lead to 'errors and biases' in earthquake studies. As will become clear, the literature on the Pohang case study has become significantly affected by such difficulties; the need is therefore to provide the means of correction.

This study will, first, summarise the different sets of magnitude determinations and b- values for earthquake populations associated with the Pohang EGS project. Next, the different magnitude determinations will be compared and causes of systematic error will be identified. To anticipate the results thus obtained, the key factors identified are, first, (A) the sparse sampling, or limited bandwidth of recording, by permanent seismograph stations in the area, and (B) miscalibration of the Sheen et al. (2018) local magnitude (M_L) scale for Korea, which affects the M_L values reported by GSK (2019) and used in subsequent publications. Second (C) is the apparent miscalibration of the formula applied subsequently by Langenbruch et al. (2020) to use these M_L values to determine magnitudes of smaller events by 'template matching'. It proves feasible to accurately quantify effects (A) and (C), but not (B); nonetheless, estimates are made of revised b- values, and revised probabilities of occurrence of any earthquake as large as M_W 5.5 are estimated.

2. Magnitudes and b-values for Pohang earthquakes

Magnitude was originally defined by Richter (1935) as a measure of

earthquake size, in terms of the logarithm of the amplitude A (in millimetres) of seismograms recorded on then-standard Wood-Anderson seismographs, with calibration for source-station distance R using an empirically-determined parameter A_O. Thus, for a given distance, a ten-fold increase in A denotes a unit increase in magnitude. The quantity so defined is now known as local magnitude, M_L. Its definition can be written as

$$M_L = \log_{10}(A) - \log_{10}(A_O(R)) + S \quad (1)$$

where S is an empirical 'station correction'. Richter (1935) calibrated this magnitude scale by specifying that A = 1 mm at a station at 100 km distance denotes $M_L = 3$, which requires $\log_{10}(A_O(R = 100\,km)) = -3$. Moment magnitude, M_W, provides an objective measure of earthquake 'size', being functionally related to the logarithm of seismic moment, M_O:

$$M_W = C + D \times \log_{10}(M_O) \quad (2)$$

where C = 9.05 and D = 1.5 (Hanks and Kanamori, 1979), independent of the characteristics of any seismograph. M_W depends on the low-frequency asymptote of the amplitude of the displacement spectrum of an earthquake, so is essentially a 'static' property, whereas M_L is more a 'dynamic' property of on earthquake, dependent on the energy radiated at higher frequencies. Deichmann (2006) showed that M_L can nonetheless serve as an equally effective measure of earthquake 'size' as M_W, provided it is determined in accordance with the Richter (1935) definition. The instrumental response of a Wood-Anderson seismograph is well quantified (e.g., Uhrhammer and Collins, 1990), enabling synthetic seismograms to be generated using records from modern digital instruments. Frequency responses of the Wood-Anderson instrument and other sensors relevant to the Pohang case study are illustrated in online supplement 2. However, for digital data to provide accurate synthetic Wood-Anderson seismograms, enabling accurate determination of M_L, the bandwidth of signal recorded must of course span that across which the earthquake radiates significant energy at frequencies to which a Wood- Anderson seismometer is sensitive. A further issue is the widespread use of proxies for M_L, such as magnitudes based on the duration (or coda length) of seismograms, or magnitudes obtained by template matching (designated here as M_T). Duration magnitudes can be determined relatively simply (e.g., Lee et al., 1972), this being the method adopted for example by the widely used HYPO71 earthquake location software. However, for each locality they require calibration against other standards (e.g., Mandal et al., 2004).

Numbers, N, of events in any earthquake population with magnitude ≥ M are expected to follow the Gutenberg-Richter law

$$\log_{10}(N(M)) = a - b\,M,\ M \geq M_C, \quad (3)$$

where a and b are constants and M_C is the 'magnitude of completeness' of the population, above which no events are missed. Populations of tectonic earthquakes usually have b ~ 1. However, in contrast, the Korean Government Commission reports on the Pohang EGS project and associated publications have determined b-values <<1. For example, Langenbruch et al. (2020) proposed b = 0.607 ± 0.068 for earthquakes associated with stimulation of well PX-2 (Fig. 4) and b = 0.762 ± 0.127 for the smaller population associated with stimulation of well PX-1. Induced earthquake populations instead typically have b > 1 (e.g., for

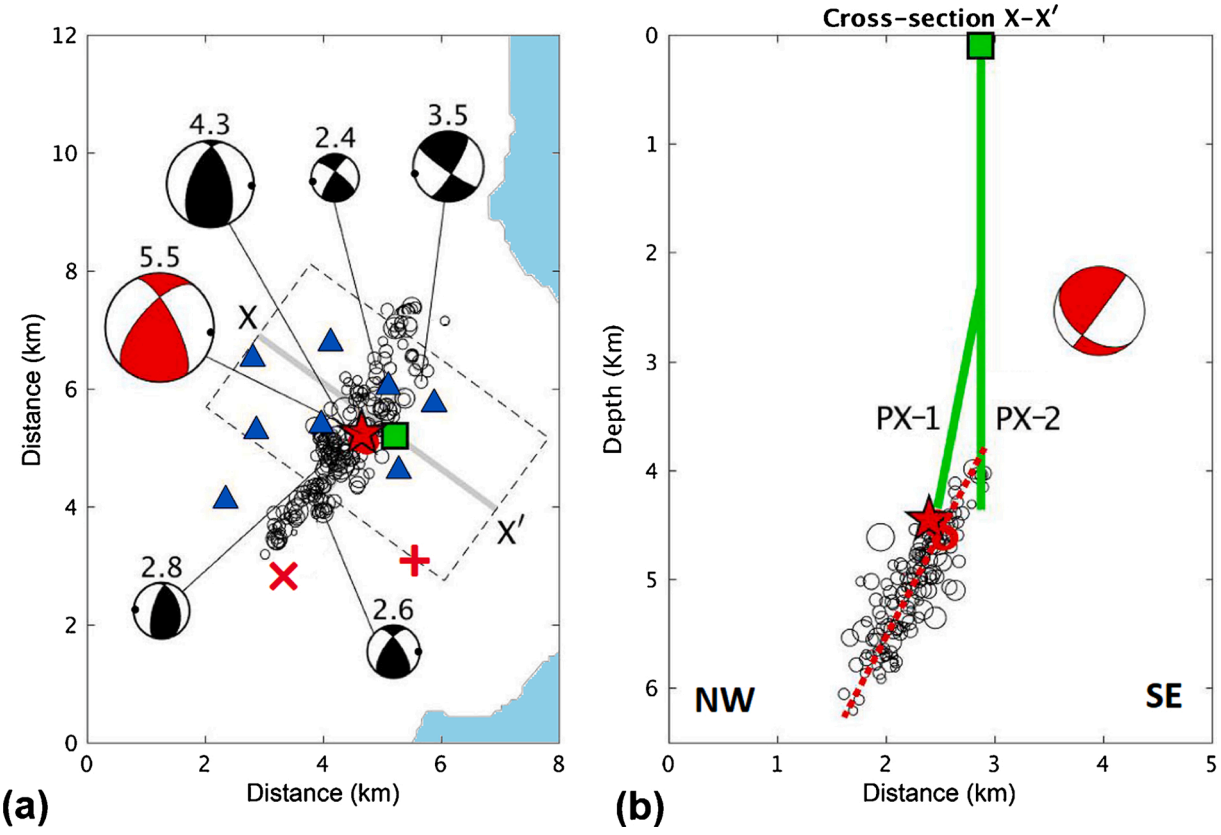

Fig. 2. (a) map, and (b) NW-SE cross-section along line illustrated in (b), showing schematically the two deep wells at the Pohang EGS site (solid green lines) and the interpreted plane of the Namsong Fault (dashed red line). Also showing locations of earthquakes at Pohang in November 2017: foreshocks (red circles); the 15 November mainshock (red star); and aftershocks (black circles), stations of the local seismograph network (blue triangles), the EGS site (green square), the thermal spa resort (red + symbol), and a borehole that yielded in situ stress measurements (red × symbol). Focal mechanisms of the mainshock and five principal aftershocks, each labelled by M_W, are drawn as standard lower (or back) focal hemisphere projections with compressional quadrants shaded. Modified from Fig. 2 of Westaway and Burnside (2019), based on Kim Kwang-Hee et al. (2018) (For interpretation of the references to colour in this figure legend, the reader is referred to the web version of this article.).

ten populations considered by Dempsey et al., 2016, b spanned 1.1–2.0 with a ~1.4 median), casting further doubt on the Langenbruch et al. (2020) analysis. Table 1 indeed lists b-values for several EGS projects. Other than for Pohang, in only one case known to me, the Habanero project in the Cooper Basin of Australia (Baisch et al., 2009), has an earthquake population from an EGS project been identified with b significantly less than 1. However, these M_L values were determined as duration magnitudes; Baisch et al. (2009) noted that they agree with M_W for the larger events in the population but are less than M_W by >1 unit for the smaller events. A b-value for this project, based on M_W values, would therefore significantly exceed the reported b-value based on duration magnitudes.

In the present study, an ensemble of potential b-values will be determined for different population subsets of N events from the Pohang earthquake dataset. These b-values are fitted by least-square regression for the events between M_C and an upper cutoff limit M_U. The regression analysis reports uncertainties (standard deviations) in the parameters a and b, as well as the overall correlation coefficient for the fit, R^2. Values of M_C and M_U were not constrained *a priori*, being instead allowed to adjust during the analysis to explore the effect of these adjustments to optimise R^2 and the uncertainty in b. In Fig. 4 it is observed that a small number of the largest earthquakes considered do not fit the determined b-value at all well. The same is evident for other subsets, to be analysed later, and provides the rationale for introducing M_U into the analysis, to avoid the risk of biasing estimates of b-values by effects of fluctuations resulting from small numbers of events at the high-magnitude ends of populations. On the other hand, many workers have taken such evidence as an indication of more complex laws than Gutenberg-Richter governing earthquake scaling (e.g., Kagan, 2002; Parsons et al., 2018; Leary et al., 2020). For example, Leary et al. (2020) have proposed that M_C values deduced from Gutenberg-Richter law fits (like that in Fig. 4) indicate a characteristic scale of inhomogeneities in hydraulic properties within the rock volume, rather than indicating incomplete recording. However, beyond noting that accurate determination of magnitudes – the aim of the present study – is needed to test such hypotheses, such considerations are beyond the scope of this study.

As will become clear, the multiple attempts at magnitude determination, some evidently more reliable than others, has become an issue for the Pohang EGS project. Ideally, an accepted magnitude standard

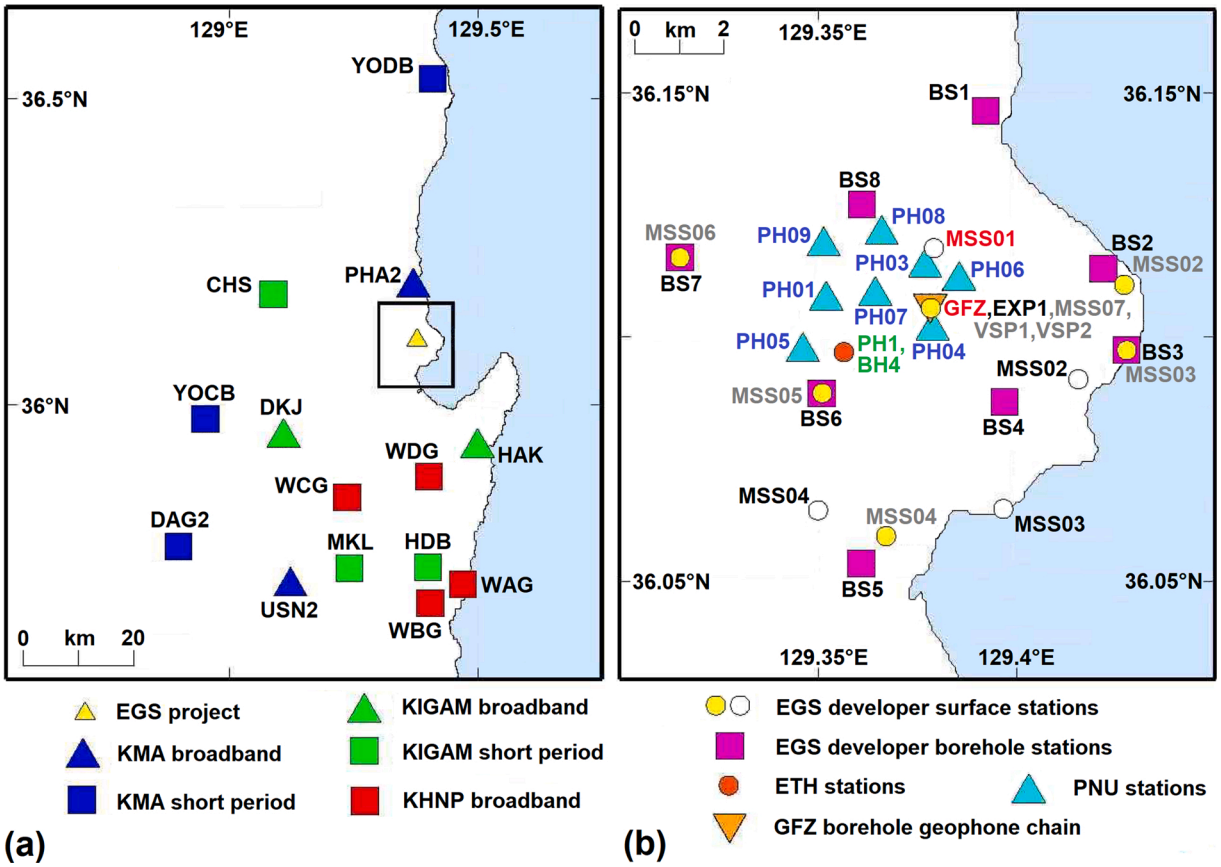

Fig. 3. Maps of seismograph stations relevant to studies of the Pohang EGS project. Summary details of these and other seismograph stations are provided by KMA (2019). Station co-ordinates are provided by Woo et al. (2019), although with some issues regarding ownership of individual stations. **(a)** Permanent regional networks operated by the Korea Meteorological Administration (KMA), the Korea Institute of Geoscience and Mineral Resources (KIGAM), and Korea Hydro & Nuclear Power (KHNP). The KHNP network monitors seismicity near the Wolseong complex of nuclear power plants to the south of Pohang. **(b)** Temporary stations installed in the vicinity of the EGS site by the developer (on whose behalf stations were operated by KIGAM), their collaborators (ETH Zürich and GFZ Potsdam, partners in the DESTRESS project), and Pusan National University (PNU) for the Kim Kwang-Hee et al. (2018) study. The PNU stations (also depicted in Fig. 2(a)) were installed in November 2019 and did not provide data during the well stimulations. Most of the developer's surface stations were relocated between stimulations to avoid noisy sites. The original sites are labelled here using fainter ornament; the same station codes were retained after the movements, creating data management issues to ensure that correct co-ordinates were used for the location of each event. These stations were a mix of velocity sensors and accelerometers, station MSS01 that (being sited on lithified bedrock) yielded the highest quality data having a Güralp CMG-40T-1 velocity sensor. The ETH accelerometer stations consisted of surface instrument PH1 and borehole instrument BH4 at ~2300 m depth. The developer's borehole instruments, BS01-BS08, in ~100–150 m deep boreholes, were also accelerometers; this category also included station EXP1 at the EGS site, which is designated as BS09 in some project documentation. The stations VSP1 and VSP2 consisted of geophones, which were installed in well PX-2 at ~1350 m and ~1550 m depths during the December 2016 stimulation of well PX-1. These instruments were lost during subsequent recovery, and so were unavailable in September 2017. Finally, the 17-instrument GFZ geophone chain was installed between depths of 1519 m and 1359 m in well PX-2 during the August 2017 stimulation of well PX-1.

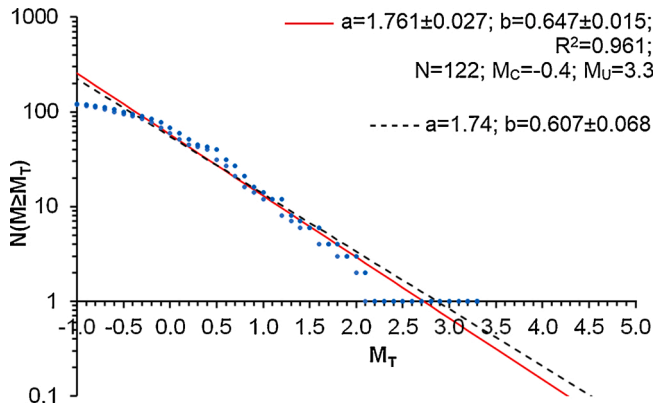

Fig. 4. Gutenberg-Richter law fits, for the earthquake population reported by Langenbruch et al. (2020), caused by stimulation of Pohang well PX-2. Magnitudes, listed here as M_T, are from 'template matching' (see text). Regression parameters, for the solid line, are from this study. Those for the dashed line, from Langenbruch et al. (2020), do not differ significantly.

Table 1
b-values for earthquake populations from geothermal projects.

Project	b	Method	Reference	Notes
Habanero, Australia	0.83	coda	Baisch et al. (2009)	1
Soultz-sous-Forêts, France	0.94	coda	Dorbath et al. (2009)	2, 3
Basel, Switzerland	1.15 ± 0.06	M_W	Bachmann et al. (2012)	4
Soultz-sous-Forêts, France	1.23	coda	Dorbath et al. (2009)	3, 5
Helsinki, Finland	1.26 ± 0.02	M_L	Kwiatek et al. (2019)	6
Puhagan, Philippines	1.27	coda	Bromley et al. (1987)	7
Paralana, Australia	1.32 ± 0.02	M_W	Albaric et al. (2014)	
Basel, Switzerland	1.58 ± 0.05	M_W	Bachmann et al. (2012)	8

A similar table to this was compiled by Bentz et al. (2020), but did not distinguish methods for b-value determination. Methods for determining magnitudes comprise duration (or coda) magnitudes, and determinations of M_W.
Notes indicate:
1, the author noted that their duration magnitudes agree with M_W for the larger events but are less than M_W by >1 unit for the smaller events. This means that a b-value based on M_W would significantly exceed the reported b-value based on duration magnitudes.
2, data for the 2003 stimulation of Soultz well GPK3.
3, duration magnitudes were calibrated as proxies for M_W.
4, earthquake population following the 2006 well stimulation at Basel.
5, for the 2000 stimulation of Soultz well GPK2.
6, the author determined this b-value using M_L. M_W is consistent with this scale for $M_W \sim 2$ but exceeds it by ~0.5 unit for M_W circa -1. This means that a b-value based on M_W would exceed the reported b-value based on M_L.
7, duration magnitudes are based on formulas derived for U.S. geothermal fields; not otherwise calibrated.
8, earthquake population accompanying the 2006 well stimulation at Basel.

would exist for the Pohang area, which could be applied to local earthquakes without contention. The natural standard here, as for anywhere equipped with modern digital seismographs, is of course M_W. However, as will also become clear, M_W has been determined for relatively few earthquakes in this area and, where comparison is possible, inconsistencies exist between determinations from different studies. In principle, as noted above, M_L might also provide a suitable standard; however, a definitive local magnitude standard for Korea has been lacking. Most countries have a single agency responsible for routine monitoring of earthquakes; for example, in the UK the BGS has this role. In the Republic of Korea this duty is split, there being two permanent national seismograph networks, operated by the Korea Institute of Geoscience and Mineral Resources (KIGAM), the national geological survey, and by KMA. KMA reports on their website (http://necis.kma.go.kr) their magnitudes, here designated as M_K, for earthquakes with $M_K \geq 2.0$; these have standing, within Korea, as 'official' indications of earthquake size. As Sheen et al. (2018) described, KMA uses a formula from Kim and Park (2002) to determine M_K, with data from their own stations, but this formula (relating seismogram amplitudes to magnitude, correcting for distance and for variations in site or path characteristics) is not defined for $M_K < 1.5$. On the other hand, as Sheen (2015) discussed, KIGAM utilises for their magnitudes a modified version of a formula originally developed for use in Japan. Sheen (2015) showed that, for each earthquake, these two magnitude values typically differ significantly; moreover, neither formula correctly captures the observed decrease in seismogram amplitudes with distance across Korea. Although the nearest permanent seismograph station was KMA station PHA2, ~10 km to the north, the next three, ~20–30 km to the south, southwest and west, were operated by KIGAM (Fig. 3(a)). The Sheen et al. (2018) magnitude scale, which set out to standardize these two pre-existing scales, will next be described. Magnitudes determined by Pohang EGS project participants will then be discussed, followed by those determined for the subsequent Commission, reported by GSK (2019) and in related publications.

2.1. The Sheen et al. (2018) M_L scale

Sheen et al. (2018) proposed a M_L scale applicable to stations of both the KMA and KIGAM networks. However, this was unavailable while the Pohang stimulations were under way in 2016–2017 and it was also not defined for the local stations deployed around the EGS site (Fig. 3(b)). Nonetheless, the Sheen et al. (2018) workflow has formed the basis for subsequent M_L determinations, so it will now be summarized. Thus, digital seismograms are de-trended, filtered with a 0.5–10 Hz, six-pole Butterworth band-pass filter to suppress microseismic noise, corrected for their own instrumental response, then convolved with the response of a Wood–Anderson instrument after Uhrhammer and Collins (1990). Regression analysis applied to the resulting amplitudes, A, resulted in formulas for the distance-dependence of amplitude for vertical and horizontal components of ground motion, subject to the assumption (after Richter, 1935) that the magnitude- dependence is on $\log_{10}(A)$ (i.e., a ten-fold increase in A represents an increase in M_L by 1). This analysis also determined a set of station corrections to M_L to account for site- or path-dependent effects, which for the vertical component of ground motion ranged from −0.29 to +0.26 at different stations.

Issues with this Sheen et al. (2018) approach, potentially limiting its usefulness, include, first, that it is only calibrated for $M_K \geq 2.0$, and, second, that its calibration utilized few data at epicentral distances of <20 km. A third difficulty is that the resulting formula for distance dependence ($A_O(R)$ in Eq. (1)) does not fit particularly well the data used to derive it, as is evident from Figures presented by Sheen et al. (2018) where the two are compared. A final issue evident from their dataset is that the resulting 'station corrections' for M_L (S in Eq. (1)) vary abruptly between adjacent seismograph stations, whereas one might expect more gradual variations, reflecting regional variations in anelastic attenuation. Nonetheless, Sheen et al. (2018) reported regression equations between magnitude scales, thus

$$M_L = 1.086\ M_W - 0.4772 \quad (4)$$

$$M_L = 0.9234\ M_K + 0.3262 \quad (5)$$

for the vertical component of ground motion. These equations imply

$$M_K = 1.176\ M_W - 0.8700. \quad (6)$$

This indicates that for larger events, M_K is a good proxy for M_W (e.g., M_K 5.0 implies M_W 4.99), but for smaller events M_K understates M_W (e.g., M_K 2.0 implies M_W 2.44). These comparisons thus indicate the extent to which M_K provides a good proxy for more familiar magnitude scales.

2.2. Magnitudes determined by EGS project participants

M_W values were determined for the August 2017 stimulation of Pohang well PX- 1, as Hofmann et al. (2019) have reported. My role in this work was to determine M_W in 'near real time' to implement the 'traffic light' protocol (after Hofmann et al., 2018; cf. Kim Kwang-Il et al., 2018) for this stimulation. To facilitate earthquake location and magnitude determination, the local station network (Fig. 3) was supplemented during this stimulation by a geophone chain, of 17 three-component geophones spaced 10 m apart, positioned between depths of 1519 and 1359 m in well PX-2 (Hofmann et al., 2019). These Sercel SGHT-15 geophones have a broadband response (see supplement 2) with a natural frequency of 15 Hz (Sercel, 2019a, b), with recording every 1 ms. A seismogram processing workstation had been established at the EGS site, using InSite software (Itasca Consulting Ltd., Shrewsbury, England) but, although events caused by the first three stimulations had been located, no M_W values had been determined; the software had rejected the amplitudes of imported seismograms as implausible, because of incorrect calibrations (conflating digital counts and volts), and so would not use them to determine M_W. This absence led to attempts to define instrument magnitudes, as will be discussed below.

As described by Itasca (2019), the InSite workflow involves direct determination of M_O by fitting low-frequency horizontal asymptotes Ω_O to displacement spectra of seismograms, corrected for instrumental response and anelastic attenuation, using the standard formula

$$M_O{}^* = \frac{4\pi\rho R V^{*3}}{F^*}\Omega_O{}^* \quad (7)$$

(e.g., Brune, 1970), where ρ is the density of rock around the seismic source, R is the source-station distance, V is the near-source seismic velocity, F is the average correction for radiation pattern, and * denotes P- or S-waves. Values of $F_P = 0.52$ and $F_S = 0.63$ are used, after Boore and Boatwright (1984). Results for each seismic phase are averaged across all reporting stations to give separate M_O determinations for P- and S-waves, M_{OP} and M_{OS}, which are combined as an overall M_O estimate, as in Table 2. Many earthquakes from previous Pohang stimulations were investigated during the setup of the correct calibrations for the instrumentation around the site (Fig. 3(b)), but in most cases the results (locations, magnitudes, focal mechanisms, etc.) were not preserved as the limitations of this software became apparent. Results have only been retained from six events, one (at 12:32 on 29 December 2016) from the first stimulation of well PX-1 and five from the second, two of which (at 04:58 and 21:42 on 13 August 2017) influenced its 'traffic light' scheme (Hofmann et al., 2019). Apart from these results, and the instrument magnitudes to be discussed below, in August 2017 the only magnitudes available were those reported by KMA for $M_K \geq 2.0$ events: at 20:31 on 22 December 2016 (M_K 2.2), 12:32 on 29 December 2016 (M_K 2.2), and 02:31 and 08:16 on 15 April 2017 (M_K 3.1 and 2.0), which are insufficient to determine a b-value. Nonetheless, the determination of $M_W = 3.18$ for the 29 December 2016 event (Table 2) is in broad agreement with the inference from Sheen et al. (2018) that, for earthquakes in this size range, M_W significantly exceeds M_K.

A major limitation of the InSite software is the manner in which it corrects for anelastic attenuation. From standard theory, if Q* is the quality factor for anelastic attenuation of seismic phase * (* = P or S), then waves of frequency f that have travelled distance R in rock with seismic velocity V* require correction by factor P* where

$$P^* = \exp\left(\frac{\pi f R}{Q^* V^*}\right). \quad (8)$$

Ideally, M_O and M_W should be determined from the displacement spectra of seismograms after separate correction of each frequency component for anelastic attenuation. However, as detailed in its technical documentation (Itasca, 2019), InSite corrects for anelastic attenuation by calculating a single value of P* for each seismic phase, at the dominant

Table 2
Earthquake source parameters using InSite.

Determinations at the Pohang EGS site in August 2017																	Hofmann et al. (2019)	
Date	Time	N_P	N_S	N (m)	E (m)	Z (m)	M_{OP} (N m)	M_{OS} (N m)	M_O (N m)	M_W	E_S (kJ)	r_P (m)	r_S (m)	R (m)	f_{CP} (Hz)	f_{CS} (Hz)	M_O (N m)	M_W
First stimulation of well PX-1																		
29 Dec. 2016	12:32:23	15	9	732	−751	3850	NR	NR	5.84×10^{13}	3.18	1.23×10^9	NR	NR	167	22.8	7.59	ND	ND
Second stimulation of well PX-1																		
11 Aug. 2017	18:50:25	17	17	−335	−107	4174	1.91×10^{10}	1.36×10^{10}	1.64×10^{10}	0.810	1.01	60.0	55.4	57.7	17.3	14.1	1.09×10^9	−0.054
12 Aug. 2017	07:06:50	17	17	−686	−663	4253	1.98×10^{10}	2.11×10^{10}	2.04×10^{10}	0.874	1.07	37.0	87.0	62.0	30.3	8.56	1.46×10^9	0.035
12 Aug. 2017	15:18:53	17	17	132	−218	4192	1.10×10^{10}	1.59×10^{10}	1.34×10^{10}	0.752	16.77	18.7	22.4	20.5	60.3	32.2	4.67×10^9	0.371
13 Aug. 2017	04:58:42	17	17	375	−320	3919	1.86×10^{11}	2.03×10^{10}	1.03×10^{11}	1.34	6440	15.1	133.6	49.6	68.2	69.8	8.08×10^{10}	1.201
13 Aug. 2017	21:42:37	17	17	−631	−448	4242	4.73×10^{11}	5.42×10^{11}	5.07×10^{11}	1.80	1.87×10^5	15.6	19.7	11.8	66.9	37.4	1.02×10^{12}	1.932

This table summarizes the earthquake source parameters that were determined using the InSite software during August 2017 and for which records were kept. Date and origin time are in Universal Time. N_P and N_S denote the number of P- and S-wave arrivals used. N, E and Z denote northward, eastward, and downward hypocentral co-ordinates relative to an origin at the PX-2 wellhead. M_{OP} and M_{OS} are estimates of seismic moment using P-waves and S-waves, M_O being the overall estimate. M_W is the corresponding moment magnitude. At the time of this work the software was set up to use Eq. (2) but with a term 9.05 rather than 9.05; this caused the resulting M_W values to be ~0.03 higher. E_S is the estimated seismic energy radiated by each earthquake; r_P and r_S are the source radius estimated from P- and S-waves, r being the overall estimate; f_{cP} and f_{CS} are the source corner frequencies for P- and S-waves. The workflow for obtaining all these values is explained by Itasca (2019) and is summarised in the main text. Values of M_O and M_W for corresponding earthquakes from Hofmann et al. (2019) are also listed. NR denotes not recorded; ND denotes not determined.

frequency of the seismometer, then scales the record of the phase by this value. For all InSite analyses, Q_P, Q_S, v_P, and v_S were set at the request of project personnel to 200, 100, 5845 m s^{-1} and 3305 m s^{-1}, respectively. For the f = 15 Hz geophone chain at R ~ 3000 m from the earthquake sources, $P_P \approx 1.13$ and $P_S \approx 1.53$. This rather naïve approach to correction for anelastic attenuation is a significant limitation of this software, which made it unsuitable for the production of definitive results. The lack of frequency-dependent correction of seismogram spectra, not amplifying high frequencies more than low frequencies, may well have affected estimation of corner frequencies, f_C, possibly explaining why these values (reported in Table 2) do not vary systematically with M_O and M_W as would be expected and are far too low for the smaller events analysed (see below); it might also have affected the fitting of horizontal asymptotes to spectra to determine M_O. The workflow might instead have adopted the estimates of Q from Kim et al. (2006) for the southern Korean Peninsula:

$$Q_P = 188.6\ f^{0.8110} \quad (9)$$

and

$$Q_S = 201.4\ f^{0.7509}. \quad (10)$$

These much higher Q values, $Q_P = 1696$ and $Q_S = 1539$ at 15 Hz, would produce M_W values lower by ~0.12. On the other hand, the adoption of $Q_P = 245$ and $Q_S = 109$ as representative of fractured granite, after Collins and Young (2000), would have produced similar M_W values to those reported. Hofmann et al. (2019) later estimated $Q_S = 200$, which for f = 15 Hz and R = 3000 m would imply P_S ~1.24 and yield magnitudes lower by ~0.06 than those reported using InSite.

The August 2017 'traffic light' protocol required actions at $M_W \geq 1.0$, ≥ 1.4, ≥ 1.7 and ≥ 2.0 (Hofmann et al., 2018, 2019). Signal amplitudes at one local surface station, MSS01 (~1.8 km north of the site; Fig. 3(b)), initiated alerts. Station MSS01 utilised a CMG-40T-1 three-component (1–100 Hz) velocity sensor (Güralp Systems Ltd., Aldermaston, England; Güralp, 2006), which has a flat response to ground velocity between frequencies of 1 Hz and 100 Hz (e.g., IRIS PASSCAL, 2020; see also supplement 2), with recording at a sampling interval of 1 ms. Data were then processed in 'near real time' to determine hypocentres, focal mechanisms, and M_O, then M_W after Hanks and Kanamori (1979) (Eq. (2). Along with smaller earthquakes, this procedure determined $M_W = 1.4$ and 1.8 for events at 04:58 and 21:42 on 13 August 2017 (Table 2). The latter event triggered a 'red' traffic- light action, ending injection and initiating flowback.

Later re-analysis of this dataset for the Hofmann et al. (2019) publication provided M_W values for 52 events (see supplement 4). As many workers (e.g., Brune, 1970; Boatwright, 1980) have demonstrated, seismic waves from earthquake sources have displacement spectra U(f) that are flat up to a corner frequency f_C, this low-frequency asymptote Ω_O being proportional to M_O, and fall off at higher frequencies f. The high-frequency decline might be in proportion to f^{-1}, f^{-2}, or f^{-3} depending on details (e.g., the ratio of rupture velocity v_R to v_S) of the source (e.g., Boatwright, 1980). Fig. 5 illustrates a model S-wave source spectrum with high-frequency f^2 dependence, after Brune (1970). The retrospective analysis by Hofmann et al. (2019) included, first, determining preliminary values of f_C for S-waves and M_O using Snoke's (1987) method. This was followed by analysis that included fitting horizontal asymptotes to S-wave spectra, as in the InSite analysis, with proper correction of spectra for anelastic attenuation, the value $Q_S = 200$ being deduced by comparing the observed high frequency decline of spectra, corrected for attenuation, with the f^{-2} dependence for Boatwright's (1978) source model. Low-frequency components were also removed from the records by applying high-pass filters, although the frequencies of these filters were not reported. This procedure yielded M_W 1.20 and 1.93, rather than 1.4 and 1.8, for the events that influenced the stimulation, suggesting consistency with the 'near real time' InSite solutions. However, as Table 2 indicates, for smaller events the Hofmann et al. (2019) M_W values diverge below the InSite values.

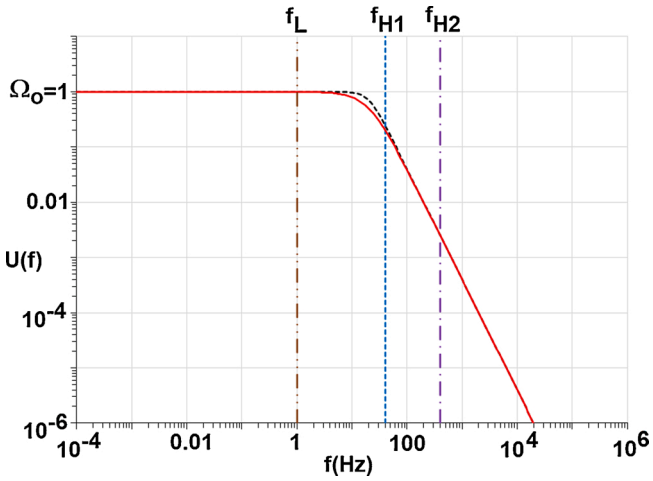

Fig. 5. Solid line is a model earthquake S-wave displacement spectrum after Brune (1970) , calculated using Eq. (22), normalized for $\Omega_O = 1$, with $f_{CS} = 20$ Hz as would be expected for M_W ~2.0. Vertical lines correspond to $f = f_L = 20$ Hz, a possible low-fequency cut-off, representing the operation of a high-pass filter, and $f = f_H = 40$ Hz and $f = f_H = 400$ Hz, high-frequency cutoffs consistent with the Nyquist frequencies of the KMA instruments at station PHA2 and the local instrument network. Dashed curve is for the alternative Boatwright (1978) source spectrum (Eq. (23)).

The Hofmann et al. (2019) earthquake population has $b = 1.12 \pm 0.03$ (Fig. 6(a)), well above the reported 0.61 ± 0.09 by Woo et al. (2019) and 0.76 ± 0.13 by Langenbruch et al. (2020) for PX-1 stimulations. If this earthquake population were to be 'compressed' into the narrower range of magnitude suggested by the InSite results (Table 2), a higher b-value would be obtained (see below). Nonetheless, b ~ 1.1 (Fig. 6(a)) (or higher) is, or would be, as expected for other EGS projects (Table 1), whereas a value as low as ~0.6 would be unprecedented. However, more significant discrepancies are evident between these magnitude determinations by the EGS project participants and those by others. Thus, for the event at 21:42 on 13 August 2017, for which InSite gave $M_W = 1.8$ and Hofmann et al. (2019) determined M_W 1.93; Lee et al. (2019) , GSK (2019), and Woo et al. (2019) reported $M_W = 1.21$ along with local magnitude $M_L = 0.67$, Langenbruch et al. (2020) also reporting $M_L = 0.67$. For the event at 04:58 on 13 August 2017, for which InSite gave $M_W = 1.4$ and Hofmann et al. (2019) determined M_W 1.20, Langenbruch et al. (2020) reported $M_L = -0.43$. In addition, the Commission report (GSK, 2019) and the derived Langenbruch et al. (2020) article, list many earthquakes with M_L circa −1 or less (Fig. 4), whereas Hofmann et al. (2019) found M_C −0.2 (Fig. 6(a)). If these M_L and M_W determinations were good proxies for each other, as would be expected if both are correctly calibrated (Deichmann, 2006), this would be surprising, as the downhole geophone chain within ~3 km of hypocentres, used by Hofmann et al. (2019), would be expected to reduce the detection threshold. Such discrepancies require resolution before any resulting b-values can be considered reliable.

As noted above, the absence of M_W values before August 2017 led to attempts to determine instrument magnitude (M_I) as a proxy for M_W or M_L. One of these, for velocity sensors, took the form

$$M_I = \log_{10}(V_M / \text{mm s}^{-1}) + 1.64 \log_{10}(R / \text{m}) + 1.92 \quad (11)$$

where V_M is peak velocity in mm s^{-1} and R is hypocentral distance. Kim Kwang-Il et al. (2018) described the process whereby another such formula was devised, starting with an equation for estimating ground motions from quarry blasts. This formula was derived using data from the February 2016 stimulation of well PX-2, but it was not presented in closed form; if this is done, one obtains

$$M_I = 0.5405 \log_{10}(V_M / \text{mm s}^{-1}) + \log_{10}(R / \text{m}) - 1.5205 \quad (12)$$

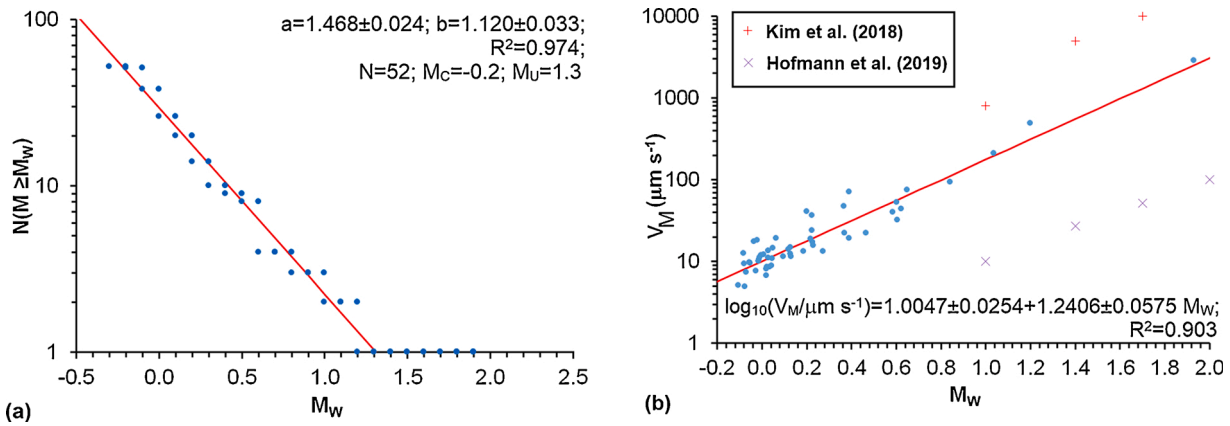

Fig. 6. The earthquake population from the August 2017 stimulation of Pohang well PX1, as reported by Hofmann et al. (2019). **(a)** Gutenberg-Richter law fit. **(b)** Peak ground velocity V_M in μm s^{-1} at seismograph station MSS01 versus M_W for the earthquakes in (a), including line fitted by least-square linear regression, for which a unit increase in M_W correlates with a ~17.4-fold increase in V_M, the parameter 1.2406 (i.e., $\log_{10}(\sim 17.4)$) being equivalent to F_T in Eq. (15). Other symbols denote estimates of V_M at station MSS01 that correspond to magnitudes 1.0, 1.4, 1.7 and 2.0 at 'traffic light' scheme thresholds: 800, 5000, 10,000 and 20,000 μm s^{-1} by Kim Kwang-Il et al. (2018) and 10, 27, 52 and 100 μm s^{-1} by Hofmann et al. (2019), these two sets of predictions differing by roughly two orders-of-magnitude.

When the Kim Kwang-Il et al. (2018) manuscript was submitted in early 2017, the intention was to use this formula to implement 'traffic light' protocols. However, such a requirement was negated with the realization, after the InSite software had been set up correctly for the August 2017 stimulation, that M_W values could be determined within ~20 min of any earthquake. GSK (2019) includes a set of 113 magnitudes listed as reported by the EGS developer between February 2016 and November 2017, 73 caused by stimulation of well PX-1 and 40 for PX-2. These M_I values were evidently based on a different formula to Eq. (12), which was not specified; M_I values for the events in common typically differ by 0.29 ± 0.06 (±s), the values from GSK (2019) being larger. Fig. 7 shows the earthquake populations thus reported by GSK (2019), b-values of 1.10 ± 0.07 and 0.97 ± 0.04 being indicated for the PX-1 and PX-2 stimulations, respectively. The $b = 1.10 \pm 0.07$ thus obtained for both PX-1 stimulations is consistent with the $b = 1.12 \pm 0.03$ obtained by Hofmann et al. (2019) for the August 2017 stimulation. However, the PX-1 earthquake population used for Fig. 7(a) only includes one event in common with Fig. 6(a), that at 21:42 on 13 August 2017, for which $M_I = 1.786$ was determined. This is in close agreement with the M_W 1.80 from InSite and M_W 1.93 from Hofmann et al. (2019), in contrast with the much lower magnitudes reported by GSK (2019); Woo et al. (2019) , and Langenbruch et al. (2020).

2.3. *Magnitudes determined by others*

Magnitudes have also been determined for earthquakes in the Pohang area by Kim Kwang-Hee et al. (2018); GSK (2019); Lee et al. (2019); Woo et al. (2019), and Langenbruch et al. (2020). However, detailed investigation is needed to understand some of these results. Some clarifications are impossible, for example Kim Kwang-Hee et al. (2018) reported that they obtained magnitudes of 150 earthquakes between November 2015 and November 2017 using 'template matching'. They illustrated these magnitudes in a diagram but did not produce a tabulation; the lack of detail makes discussion impossible.

The procedure adopted by GSK (2019) for magnitude determination is key to the work that has followed, and the resulting criticism of Pohang EGS project personnel for not anticipating the magnitude 5.5 earthquake, but was not clearly explained. A paraphrase of this workflow, edited for translation and language difficulties, and with excision of unnecessary material, is provided in supplement 1. In summary, they started by assembling an initial catalogue of 520 earthquakes in the wider Pohang area, then applied a procedure like that of Sheen et al. (2018) to 194 events near the EGS site between 16 November and 31 December 2017 to determine a set of station corrections S (cf. Eq. (1)) to M_L for the KMA and KIGAM permanent stations and for the temporary local network stations (Fig. 8). The earthquakes used for this analysis were not reported; however, the KMA archive lists 48 events in the area

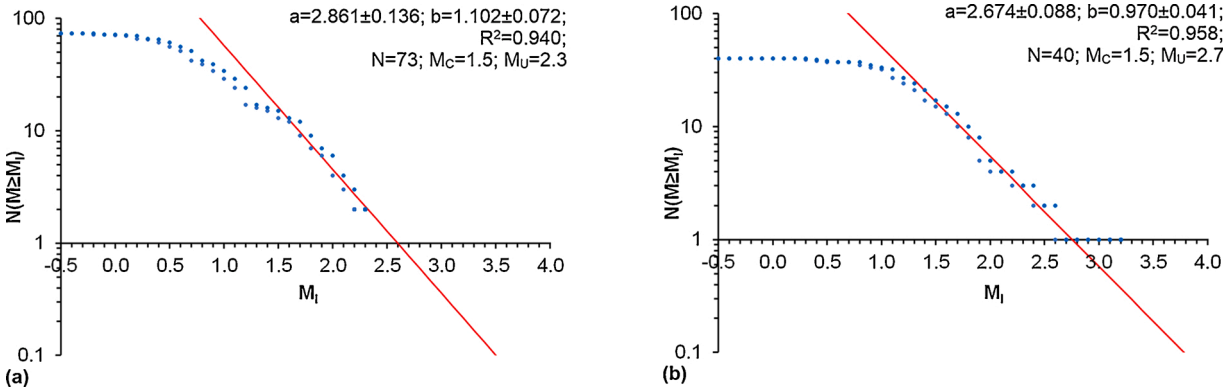

Fig. 7. Gutenberg-Richter law fits for the earthquake populations from Pohang well stimulations, as reported by the EGS developer for GSK (2019). **(a)** For well PX-1. **(b)** For well PX-2.

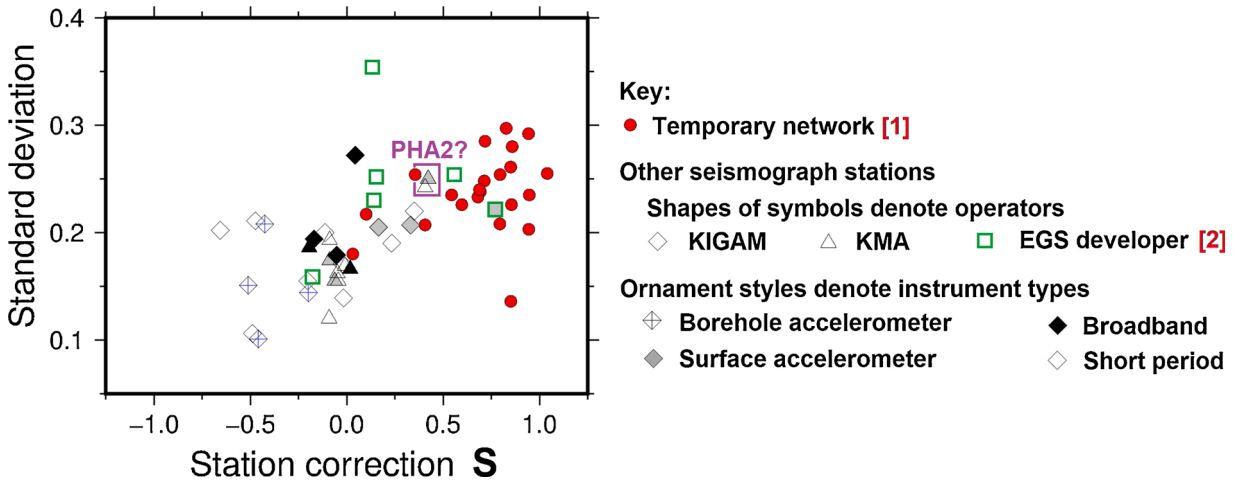

Fig. 8. Comparison of the station corrections S (cf. Eq. (1)) as measured for each seismograph station in the Pohang area (Fig. 3), for a set of 194 earthquakes between 16 November and 31 December 2017, as reported by GSK (2019) (their Fig. 5–7; see supplement 1). For each station that yielded data, the mean of S is plotted against the associated standard deviation. This diagram reports that the KMA and KIGAM stations have small S, but the 22 'temporary network' [1] and 6 'EGS developer' [2] stations typically have large positive values. Overall, these 28 stations appear to correspond to those in Fig. 3, thus: the seven surface stations and nine borehole stations operated by KIGAM on behalf of the developer, NexGeo; the two VSP stations; the two stations provided by ETH Zürich as part of collaboration; and the eight stations provided by PNU (although note the mismatches between instrument types at some stations reported by GSK, 2019, between here and in Fig. 3.). Although no stations were identified individually in the original diagram, the points that most likely correspond to station PHA2 have been labelled.

with $M_K \geq 2.0$ during this time span, so most of those utilized must have been smaller. The station corrections obtained by GSK (2019) (Fig. 8; see supplement 4 for more details) range from +1.0 to −0.2 for the local stations, being positive for all but one station, and from +0.4 to −0.6 for the permanent stations, these latter corrections having been determined such that they average to zero. Weighting each data point equally, the mean values of S in Fig. 8 are 0.60 ± 0.14 for the temporary stations and -0.09 ± 0.11 for the permanent stations (both ±2 s), the two medians being 0.71 and −0.07. GSK (2019), like Sheen et al. (2018), attributed this range of station corrections to variations in site conditions. However, as will become clear below, it is suggested instead that this pattern is evidence of systematic errors in M_L caused by miscalibration of A_O in the Sheen et al. (2018) formula and the effect of f_C being high relative to the Nyquist frequency f_N at the permanent stations for the small earthquakes analyzed. The Nyquist frequency is the highest frequency of signal that can be recorded without distortion through aliasing, being half the reciprocal of the sampling interval. GSK (2019) then determined M_L using the Sheen et al. (2018) procedure, applied to data from stations of both the permanent and temporary networks, with their new set of station corrections, so determining M_L for 40 earthquakes, being limited by the difficulty of convolving the Wood-Anderson seismograph response. To create a larger dataset, they used the peak amplitudes of the accelerometer and seismometer records, A_M and V_M, at KMA station PHA2 for these 40 earthquakes to calibrate prediction equations for proxy values for M_L, here designated as M_P. The equations thus obtained, which were not reported by GSK (2019), are

$$M_P = 3.765 + 1.117 \log_{10}(V_M / \text{mm s}^{-1}) \quad (13)$$

and

$$M_P = 1.576 + 1.152 \log_{10}(A_M / \text{mm s}^{-2}). \quad (14)$$

These equations lack distance-dependence, so are only applicable for the ~10 km distance from the subsurface beneath the EGS site to PHA2; they enabled GSK (2019) to determine M_P for additional earthquakes. GSK (2019) also reported M_W determinations, which they stated were carried out in the time domain on P-wave records, except for the 15 November 2017 mainshock where a frequency-domain technique on P-waves was used. Thus, overall, GSK (2019) reported a catalogue of 98 earthquakes between November 2015 and 15 November 2017, all with epicentres within ~0.5 km of the EGS project site, with M_W values for 46 of these events. As is detailed in supplement 4, one additional event (at 03:58 on 31 March 2016) seems to have been omitted from this catalogue by mistake; its re-inclusion increases this population to 99 events. For 40 of these events, M_L was reported after Sheen et al. (2018); for the others M_P was determined using one of the prediction equations, although GSK (2019) did not indicate which method yielded which magnitudes.

Fig. 9(a) shows a Gutenberg-Richter fit for these 99 events, fitted with $b = 0.64 \pm 0.02$, similar to the value deduced by GSK (2019) for the same population (see supplement 1). Although listed as M_L, as noted above, this set of magnitudes is a mix of 'true' M_L values, from synthesizing Wood-Anderson seismograms, and values of M_P. Fig. 9(b) shows the fit with $b = 0.82 \pm 0.05$ for the 47 events for which M_W was determined. Fig. 9(c) shows the fit to M_W for the 39 events with 'true' M_L values, likewise fitted with $b = 0.90 \pm 0.10$, although with a higher threshold of completeness, M_L 1.6 versus M_W 1.3. This mismatch is reflected in Fig. 9(d), which shows that, for the events in common between parts (b) and (c), M_W diverges above M_L for $M_L < 1.5$. A similar graph to Fig. 9(d) was plotted by GSK (2019) (see supplement 1); although it illustrates the same mismatch between M_W and M_L this graph was used to infer that these values are well-correlated and thus mutually consistent. Another mismatch is between the value $M_W = 1.93$ reported by Hofmann et al. (2019) for the event at 21:42 on 13 August 2017, for which GSK (2019) determined $M_L = 0.67$ and $M_W = 1.21$. Clearly, if the Hofmann et al. (2019) magnitude is correct, the GSK (2019) values have been underestimated, M_L more so than M_W. If so, the GSK (2019) earthquake population in Fig. 9 would become 'compressed' into a smaller range of magnitudes, increasing its b-value.

Again with the 31 March 2016 03:58 event reinstated, Woo et al. (2019) reported the same 99 M_L and 47 M_W determinations. They acknowledged Korean Government Commission funding but did not cite Lee et al. (2019) or GSK (2019); their work was presented as an original study rather than as a summary of a wider investigation already published. They explained that for 40 events they determined M_L by synthesizing Wood-Anderson seismograms and applying the Sheen et al. (2018) M_L formula with modified station corrections; they listed these 40 events (including the mainshock) in their supplementary Table S2 (see supplement 4). Woo et al. (2019) briefly discussed the station corrections they obtained, which differ in detail from those reported by GSK (2019); this is puzzling, because it is now clear that the same workflow is

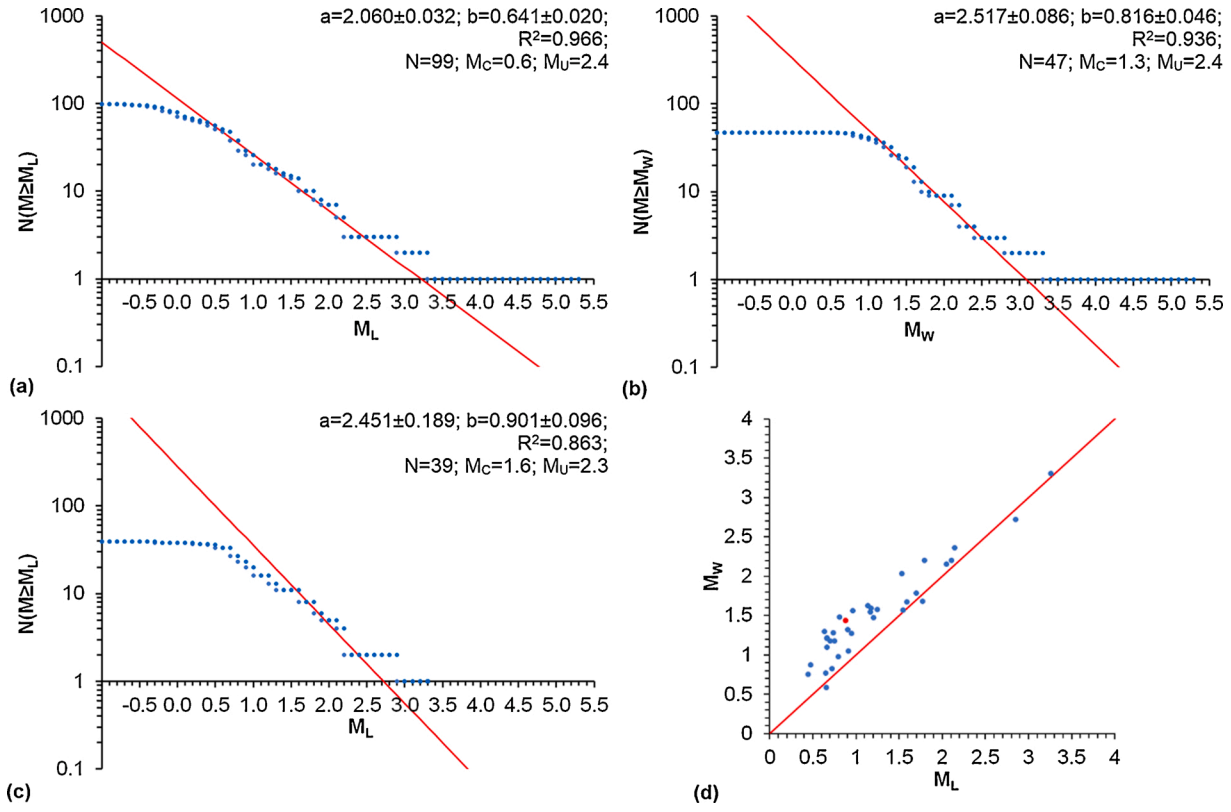

Fig. 9. Earthquake populations reported by GSK (2019). **(a)** 'M_L values' (in reality, a mix of M_L and M_P values; see supplement 4) for their population of 99 earthquakes near the Pohang EGS site. These are modelled with a Gutenberg-Richter law fit that is similar to the fit with a = 2.0 and b = 0.73 determined for the same earthquakes by GSK (2019) (see supplement 1). **(b)** Gutenberg-Richter law fit for the 47 events in the population in (a), for which GSK (2019) determined M_W values. **(c)** Gutenberg-Richter law fit for the 39 events in the population in (a), for which GSK (2019) determined M_L values using synthetic Wood-Anderson seismograms (as opposed to using one of their empirical prediction equations). **(d)** Scatter graph of M_W against M_L for the 35 events in common between the populations in (b) and (c) (excluding the 15 November 2017 mainshock), with line for $M_W = M_L$, highlighting the event at 21:42 on 13 August 2017.

being reported. Woo et al. (2019) indeed noted that the temporary stations typically required large positive station corrections, up to +1.177, which they too attributed to site amplification caused by unconsolidated rocks. For the other 59 events, Woo et al. (2019) stated that they determined magnitudes from the peak amplitudes of S-waves recorded at station PHA2 but without any clear explanation of the method. The resulting magnitudes are identical to those determined by GSK (2019); the method must thus have been the same, and must therefore have used the prediction equations from GSK (2019), although these were not mentioned by Woo et al. (2019). The 99-event Woo et al. (2019) catalogue is thus a mix of M_P and 'true' M_L values, all reported as M_L. Two of their 47 M_W values were determined in the frequency-domain using seismograms from PHA2: S-wave spectra for the mainshock ($M_W = 5.56$); and P-wave spectra for the largest event during the stimulations, at 02:31:13 on 15 April 2017 (M_W 3.29). The other 45 (reported as M_W 0.58–2.72) were by time-domain integration of P-wave signals, after Tsuboi et al. (1995) and Prejean and Ellsworth (2001) , again using PHA2 data. Although this explanation differs somewhat from GSK (2019), the resulting M_W values are exactly the same. Woo et al. (2019) used their M_L and M_P values to determine b-values: 0.66 ± 0.08 overall, 0.65 ± 0.09 for PX-2 stimulation, and 0.61 ± 0.09 for PX-1 stimulation. For the event at 21:42 on 13 August 2017 Woo et al. (2019) reported $M_L = 0.67$ and $M_W = 1.21$, the latter value determined in the time domain, both well below the $M_W = 1.93$ from Hofmann et al. (2019).

Langenbruch et al. (2020) reported a 234-event catalogue spanning February 2016 to November 2017. They stated that to ensure reliable b-values they used a uniform catalogue of M_L values, but this is not so. Their catalogue includes the $M_W = 5.5$ mainshock and 39 of the 40 events for which Woo et al. (2019) reported 'true' M_L values, all with the same M_L values, plus the 59 events that yielded their M_P values, plus 137 'extra' events. Of these 137 events, 17 were in the initial 520 event GSK (2019) catalogue but not in their final 99 event catalogue, and are listed with M_P values determined by GSK (2019); the remaining 119 are 'new'. For each of the latter 195 events (i.e., 59 + 17 + 119), Langenbruch et al. (2020) reported magnitudes M_T determined by template matching seismograms from PHA2. Peng and Zhao (2009) explained that this technique matches windowed seismograms to records of previously located events. If a match that meets specified correlation criteria is achieved, the hypocentres must be close or identical. M_T for the detected event is then determined from the median of the ratios of maximum amplitudes between the template and detected events, for all components of ground motion recorded, assuming that a tenfold increase in amplitude corresponds to a unit increase in magnitude. Langenbruch et al. (2020) thus, effectively, used the formula

$$M_T = M_{LT} - \frac{\log_{10}(A_L/A_T)}{F_T} \quad (15)$$

where M_{LT} is M_L for whichever template event was used to determine each M_T value, A_L/A_T is the S-wave amplitude-ratio at PHA2 for the two events, and the scale factor F_T is set equal to 1. However, Langenbruch et al. (2020) did not state which template event was used to determine M_T for which other events, and it is not possible to establish this from their table of results (which might have been simply modified to identify, for each M_T value, the event that provided its 'template'). Although, for a given hypocentral distance, the equivalence of a tenfold increase in amplitude to a unit increase in magnitude (i.e., $F_T \equiv 1$) is the basis of the Richter (1935) definition of M_L, this applies to amplitudes measured (or

synthesized from digital records) on a Wood-Anderson seismograph, not raw records from other types of instrument; there is no basis for this assumption for seismograms in general. Nonetheless, as Fig. 10 shows, there is overall no systematic difference between these M_T values and the M_P values from GSK (2019), although for some events these values differ by up to ~0.2. However, for the event at 04:58 on 13 August 2017, which caused the 'amber' traffic light action during stimulation of well PX-1, Langenbruch et al. (2020) reported $M_T = -0.42$, well below the $M_W = 1.20$ determined by Hofmann et al. (2019), another substantial discrepancy.

3. Reconciling inconsistencies in magnitudes

It is clear from the foregoing summaries that significant discrepancies exist between magnitude determinations for Pohang earthquakes by different workers. Of the analyses, the Hofmann et al. (2019) study stands out as having a straightforward workflow using established methods, there thus being no reason to question its findings. Each of the other sets of results has resulted in lower magnitude values, whether M_W, M_L or the M_P and M_T proxies for M_L. This is despite the expectations that if M_L is correctly calibrated it should agree with M_W (e.g., Deichmann, 2006) and that different methods for M_W should yield consistent results, so the time-domain technique used by GSK (2019) and Woo et al. (2019) should be consistent with the frequency-domain techniques used by Hofmann et al. (2019). However, it is also clear that GSK (2019); Woo et al. (2019), and Langenbruch et al. (2020), have determined mutually consistent results for larger events, with magnitudes >2, these latter results also agreeing with the magnitudes determined by KMA. Clearly, if these latter studies have determined correct magnitudes for the larger events and have underestimated magnitudes for the smaller events, their catalogues of events have become 'stretched' into ranges of magnitude that are too large. If these results are corrected by 'compressing' them back into smaller magnitude ranges, the b-values will increase; the unprecedentedly low b-values determined by GSK (2019); Woo et al. (2019) , and Langenbruch et al. (2020) might thus be interpreted as evidence of magnitude miscalibration. An additional reason

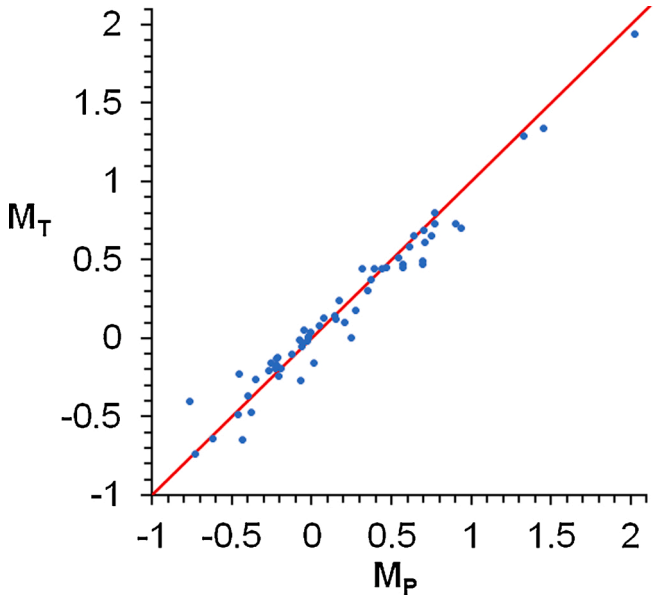

Fig. 10. Comparison of magnitudes M_P determined by GSK (2019) using their prediction equations based on seismogram amplitudes versus magnitudes M_T determined by Langenbruch et al. (2020) using their template matching method, also based on seismogram amplitudes. The limited scatter about the line $M_T = M_P$ indicates that these two methods produce similar results, even though (as is discussed in the text) different dependence of magnitude on amplitude is assumed for the two methods.

for suspecting miscalibration arises from the completeness thresholds of earthquake populations. The Langenbruch et al. (2020) population for stimulations of well PX-2 has M_C −0.4 (Fig. 4), whereas that from Hofmann et al. (2019) for the August 2017 stimulation of well PX-1 has M_C −0.2 (Fig. 6(a)). The Hofmann et al. (2019) study used data from the aforementioned geophone chain positioned in well PX-2 at a depth of ~1.5 km, so ~3 km from the hypocentres, whereas Langenbruch et al. (2020) used data from station PHA2, ~10 km away. Even allowing for the fact that PHA2 is a well-sited permanent seismograph station, it seems unlikely that it might record smaller earthquakes than could be detected by the geophone chain at much shorter distances. The present analysis will proceed, first, by attempting to reconcile the InSite M_W values (Table 2) with the M_W values reported as definitive by Hofmann et al. (2019). The results of GSK (2019); Woo et al. (2019), and Langenbruch et al. (2020) will then be assessed. Before these comparisons are reported, key aspects of theory will be summarized.

First, the potential effect of miscalibration of values of some magnitude scale, meaning 'uncorrected' values M_U calculated using the formula

$$M_U = M_R - \log_{10}(V_M/V_{MR}), \tag{16}$$

where V_M is the maximum amplitude of a seismogram of the event, and M_R is the known magnitude of a co-located 'template event' for which the maximum amplitude of the seismogram is V_{MR}, may be estimated as follows. The 'amended' value M_A is intended to provide a true proxy for magnitude below some threshold M_R, with

$$M_A = M_R - \Gamma \log_{10}(V_M/V_{MR}) \tag{17}$$

and Γ a constant. It follows that

$$M_A = (1 - \Gamma)\, M_R + \Gamma\, M_U. \tag{18}$$

Second, consideration of earthquake source theory is also required. Thus,

$$M_O = \frac{16}{7}\Delta\sigma r^3 \tag{19}$$

(after Eshelby, 1957) with Δσ the coseismic stress drop and r the radius of the earthquake source. This formula assumes the ratio of seismic velocities $V_P/V_S = \sqrt{3}$ (i.e., Poisson's ratio 0.25); formulas for more general rock properties are available (e.g., Westaway and Younger, 2014). Many workers have modelled earthquake sources with flat displacement spectra below a corner frequency f_C, above which spectral displacement tails off (e.g., Brune, 1970; Sato and Hirasawa, 1973; Madariaga, 1976; Kaneko and Shearer, 2014; Madariaga and Ruiz, 2016). In general,

$$f_C{}^* = \frac{k^* V_S}{r} \tag{20}$$

where * denotes P- or S-waves. Combining these formulae gives

$$f_C{}^* = k^*\, V_S \left(\frac{16\Delta\sigma}{7\mathrm{Mo}}\right)^{1/3}. \tag{21}$$

For the Pohang granite, $V_S = 3305$ m s^{-1} (Hofmann et al., 2019) or 3310 m s^{-1} (Woo et al., 2019). GSK (2019) and Woo et al. (2019) determined $\Delta\sigma = 5.6$ MPa for the 15 November 2017 Pohang mainshock; the latter study assumed the same value for smaller events.

This theory can be applied, using $\Delta\sigma = 5.6$ MPa and $V_S = 3305$ m s^{-1}, with $k_P = 0.38$ and $k_S = 0.26$ for sources that rupture at speed $V_R = 0.9\, V_S$ (Kaneko and Shearer, 2014); results in the range M_W −1 to 3 are listed in Table 3. Thus, f_{CP} and f_{CS} range from 8.9 and 6.1 Hz for $M_W = 3$ to 894 Hz and 612 Hz for $M_W = -1$. Values from Kwiatek and Ben-Zion (2016) are also included, for comparison. Other studies propose higher k_P and k_S, for example Sato and Hirasawa (1973) reported $k_P = 0.42$ and $k_S = 0.29$ for $V_R = 0.9\, V_S$. Higher values also arise for

Table 3
Corner frequency variations.

		Kwiatek and Ben-Zion (2016)		This study				
M_W	M_O (N m)	f_{CP} (Hz)	f_{CS} (Hz)	f_{CP} (Hz)	f_{CS} (Hz)	Ψ [1]	Ψ [2]	Ψ [3]
3.0	3.55×10^{13}	9.3	10.0	8.9	6.1	0.934	0.943	0.916
2.5	6.31×10^{12}	16.7	17.8	15.9	10.9	0.893	0.907	0.859
2.0	1.12×10^{12}	29.6	31.3	28.3	19.3	0.766	0.785	0.737
1.5	2.00×10^{11}	52.3	56.1	50.3	34.4	0.644	0.641	0.589
1.0	3.55×10^{10}	92.3	98.8	89.4	61.2	0.405	0.370	0.363
0.5	6.31×10^{9}	163	184	159	109	0.298	0.263	0.239
0.0	1.12×10^{9}	317	301	283	193	0.154	0.129	0.148
−0.5	2.00×10^{8}	516	705	503	344	0.115	0.096	0.086
−1.0	3.55×10^{7}	809	1239	894	612	0.064	0.053	0.048

M_W is moment magnitude, M_O is seismic moment, and f_{CP} and f_{CS} are the P-wave and S-wave corner frequencies. M_O is determined from M_W using Eq. (2). Calculations of f_{CP} and f_{CS} from Kwiatek and Ben-Zion (2016) assume $\Delta\sigma = 10$ MPa, and $V_S = 2887$ m s^{-1}, for earthquake sources that rupture at speed $V_R = 0.9\ V_S$, Kwiatek and Ben-Zion (2016) stated that they used input parameters that correspond to $k_P/k_S = f_{cP}/f_{cS} = 1.39$; however, for reasons that are not apparent, their values of f_{cP} and f_{cS} are not consistent with this ratio. Calculations of f_{CP} and f_{CS} for this study apply Eq. (21) using $\Delta\sigma = 5.6$ MPa and $V_S = 3305$ m s^{-1}, with $k_P = 0.38$ and $k_S = 0.26$, likewise for $V_R = 0.9\ V_S$ (after Kaneko and Shearer, 2014); these values result in $k_P/k_S = f_{cP}/f_{cS} = 1.46$, as listed. The parameter Ψ is defined in the text (cf. Fig. 15). For each value of M_W: Ψ [1] is for a Brune (1970) source spectrum; Ψ [2] is for a Boatwright (1978) source spectrum; and Ψ [3] is for a Brune (1970) source spectrum multiplied by the frequency response of a Wood-Anderson seismograph (after Uhrhammer and Collins, 1990).

$V_R > 0.9\ V_S$; for example, the Brune (1970) source model, which assumes instantaneous rupture, has $k_S = 0.37$. Furthermore, the aforementioned values are averaged over the focal sphere; Kaneko and Shearer (2014) reported that, for $V_R = 0.9\ V_S$, k_P and k_S peak at 0.73 in some directions, which would indicate $f_{CP} = f_{CS} = 54$ Hz for $M_W = 2.0$.

3.1. Reconciling InSite and Hofmann M_W values

As already noted, the M_W values reported by Hofmann et al. (2019) obtained in the field using InSite and via the retrospective analysis are consistent for $M_W > \sim 1$ but diverge for smaller events; for the smallest events in common, InSite yielded $M_W \sim 0.8$ for events for which the retrospective analysis yielded $M_W \sim 0$. This divergence must reflect the differences in procedure for the two sets of M_W determinations.

The first difference arises from consideration of anelastic attenuation. As already noted, InSite determined this effect as $P_S \approx 1.53$ for a 15 Hz S-wave travelling a distance of 3000 m with $Q_S = 100$. Previous discussion indicated that this value of Q_S was too low. Given the manner (already described) in which InSite corrects for anelastic attenuation, if no correction had been applied, then M_O values would scale to $1/P_S$ or ~0.65 of their calculated values; from Eq. (2) this would reduce M_W by ~0.28. A second issue, noted by Hofmann et al. (2019), is that the InSite analysis only used direct P- and S-wave arrivals, whereas the subsequent analysis also used phases that entered the open-hole section at the base of well PX-2 and travelled up this well as Stoneley waves (or 'tube waves'); this latter set of locations is, thus, more accurate. Comparison of Table 2 with the hypocentral locations from Hofmann et al. (2019) indicates that the InSite locations are typically deeper, by ~100 m or so. Adjustment of these sources closer to the recording stations by this distance would reduce the corrections for geometric spreading and anelastic attenuation, but the effect would be small, <0.1 in terms of M_W.

The differences between the InSite and retrospective magnitudes must therefore primarily relate to the high-pass filtering of the seismograms, of the smaller events, by Hofmann et al. (2019). Although these authors did not disclose filter parameters, these must have affected frequencies of up to several tens of hertz to remove the frequency components that resulted in the 'false' corner frequencies and overestimations of M_O by the InSite analysis. The use by Hofmann et al. (2019) of the Snoke (1987) method to obtain mutually-consistent preliminary values of M_O and f_{CS} (which was not possible using InSite) was evidently beneficial to the accuracy of their retrospective analysis.

The frequency components that were removed from the August 2017 seismograms by the Hofmann et al. (2019) high-pass filtering might in principle relate either to meteorological effects (e.g., wave action in the nearby sea) or to anthropogenic 'cultural noise'. The August 2017 well stimulation roughly coincided with one of the largest typhoons to affect Korea, the category 4 Typhoon Noru, which caused heavy rainfall at the site for days on end. However, this typhoon passed Korea and was already waning by 8 August (Gutro, 2017), several days before the earthquakes under scrutiny (Table 2). Furthermore, the microseismic noise caused by ocean waves is concentrated circa 0.1–0.5 Hz (e.g., Longuet-Higgins, 1950; Sheen et al., 2009). It thus seems more likely that the cause was 'cultural noise'. In the Pohang area this might have had many sources, such as road traffic (a motorway runs past the site compound), railways (a high speed railway line, much of it in tunnels, is nearby), or the nearby port and steelworks complex (cf. Sheen et al., 2009; Lecocq et al., 2020). Significant effects of high-frequency 'cultural noise' have been demonstrated for borehole seismometers elsewhere (e.g., Young et al., 1996; Boese et al., 2015), as well as for surface instruments. The potential impact of the frequency content of 'cultural noise' on the ability to analyse earthquakes at this site (whether using data from temporary local stations or the permanent regional networks) was not considered during the August 2017 stimulation and seems not to have been addressed by the subsequent Commission.

3.2. Reconciling EGS participant magnitudes with Woo et al. (2019) and Langenbruch et al. (2020)

Again, as already noted, there are also major discrepancies between the magnitudes reported by the EGS project participants and those reported by Langenbruch et al. (2020). In summary, for the event at 04:58 on 13 August 2017, which caused the 'amber' traffic light action during stimulation of well PX-1, Woo et al. (2019) and Langenbruch et al. (2020) reported $M_T = -0.42$, well below the $M_W = 1.20$ determined by Hofmann et al. (2019) and M_W 1.4 reported using InSite. For the event at 21:42 on 13 August 2017, which caused the 'red' traffic light action, Lee et al. (2019) and Woo et al. (2019) reported $M_W = 1.21$ and $M_L = 0.67$, well below the $M_W = 1.93$ determined by Hofmann et al. (2019) and the M_W 1.8 using InSite. Langenbruch et al. (2020) repeated this $M_L = 0.67$ value and used it for this event, as one of their 'template events', for determining magnitudes of smaller events. These discrepancies greatly exceed those discussed in the preceding section, which only arose for the smallest events studied.

Key to reconciling such discrepancies, it is suggested, are the low sampling intervals of the permanent stations that reported the data used by Lee et al. (2019); Woo et al. (2019) and Langenbruch et al. (2020). In August 2017, station PHA2 was equipped with both velocity seismometers and accelerometers (cf. KMA, 2019). The three-component Güralp CMG-40T-1 sensor (Güralp Systems Ltd., Aldermaston, England; Güralp,

2006) has a flat response to ground velocity over 1–100 Hz (e.g., IRIS PASSCAL, 2020; see supplement 2). The three-component Kinemetrics EpiSensor EST accelerometer (Kinemetrics, Inc., Pasadena, California) has a flat response to ground acceleration up to 200 Hz (Kinemetrics, 2017; see also supplement 2). These instruments were interfaced to a Kinemetrics Quanterra Q330S recording system (Kinemetrics, 2019), which was set to record all six data channels with 100 samples per second. In this configuration, the Nyquist frequency was 50 Hz; an abrupt anti-aliasing filter was therefore applied to strongly attenuate signals above ~40 Hz (e.g., Ahern and Dost, 2006; Quanterra, 2007). Conversely, as already noted, the Pohang local network and downhole geophone chain recorded every 1 ms, with a 500 Hz Nyquist frequency.

Taking account of these considerations, in addition to the empirical correction approach represented by Eq. (18), a second method for magnitude correction can also be devised, taking into account the form of earthquake source spectra (Fig. 5). Brune's (1970) earthquake source theory predicts S-wave displacement spectra U(f), of the form

$$U(f) = \Omega_O \frac{1}{1 + f^2/f_C^2} \tag{22}$$

which behaves as f^{-2} at high frequencies (Fig. 5). Boatwright's (1978) alternative source model,

$$U(f) = \Omega_O \frac{1}{\left(1 + f^4/f_C^4\right)^{1/2}} \tag{23}$$

has similar form, but a sharper 'corner' around f_C (Fig. 5), and can be used to test whether conclusions reached are sensitive to the precise form of source spectra. Representative values of f_{CP} and f_{CS}, for P- and S-waves, as functions of M_W and M_O, are listed in Table 3.

If an earthquake with P- or S-wave spectra of the form of Eq. (22) or (23) were to be recorded by an instrument whose sensor cuts off, due to anti-alias filtering, at a relatively low frequency f_H (say, $f_H = 40$ Hz), part of the signal would be lost, whereas if f_H were much higher (say, 400 Hz), the loss would be less significant, potentially negligible. As others (e.g., Kwiatek and Ben-Zion, 2016) have noted, the seismograms recorded with low f_H, which might be envisaged as Fourier transforms of such spectra, are thus expected to have smaller amplitudes, which decrease progressively from the condition for recording with $f_H \approx f_C$ to that with $f_H << f_C$, relative to $f_H >> f_C$, providing a natural explanation for the underestimation of magnitudes based on records from stations with low f_H, such as PHA2. On this basis, the underestimation would affect any magnitude that depends on records in the time-domain. This would include, first, M_L values, based on synthesizing records from Wood-Anderson seismographs, determined by GSK (2019) and reported by Woo et al. (2019) and Langenbruch et al. (2020). Second, it will include most of the M_W values determined by GSK (2019) and reported by Woo et al. (2019) and Langenbruch et al. (2020), as these were based on time-domain methods. Finally, it will affect the M_P values reported by these studies, which were based on comparison of seismogram amplitudes with prediction equations referenced to M_L, and the M_T values determined by Langenbruch et al. (2020) using 'template matching' relative to M_L values, since the underlying M_L values would themselves be subject to systematic error.

The importance of this effect can be investigated by comparing the amplitudes of synthetic seismograms generated for earthquakes with a given M_W, with and without frequency truncation. In principle, many versions of software are available for doing this (e.g., Frankel, 2009; D'Amico et al., 2017). Such software works stochastically, assuming random phase variations between frequency components based on the properties of random noise, following a general method originally developed by Boore (1983) . However, Boore (1983) pointed out that for earthquakes with $M_W \leq 3$, predictions assuming stochastic phase variations and assuming coherent sources, with all frequency components in phase, have very similar amplitudes. As others (e.g., Westaway and Younger, 2014) have noted previously, calculations for earthquakes in this size range assuming coherent sources are much simpler to implement. This effect is thus investigated in the present study by generating 'synthetic seismograms' as inverse Fourier transforms of a coherent model source spectrum. Details of the method used are explained in supplement 3. This method determines, as functions of M_W, values for a parameter Ψ that estimates the ratio of seismogram amplitudes with and without spectral truncation. Table 3 indicates that $\Psi \to 0$ at very small M_W and $\Psi \to 1$ at large M_W. A continuous empirical function that might approximate this behaviour is

$$\Psi(M_W) = \frac{\alpha}{2}(\tanh(\beta(M_W - M_{WO}) + 1) + \frac{(1-\alpha)}{2}\left(\frac{2}{\pi}(\arctan(\gamma(M_W - M_{WO})) + 1\right) \tag{24}$$

where α, β, γ and M_{WO} are parameters, adjustable to cover variants of the analysis relating to different source models or instrumental response. Given the definition of Ψ and the original Richter (1935) definition of M_L, the resulting correction to M_L, ΔM_L, can be expressed as

$$\Delta M_L = -\log_{10}(\Psi), \tag{25}$$

ΔM_L being positive because $0 < \Psi < 1$. Fig. 11 illustrates the variations of Ψ with M_W, assuming Brune (1970) and Boatwright (1978) source spectra (unmodified for effects of anelastic attenuation or instrumental response) and assuming the Brune (1970) spectrum with a Wood-Anderson instrumental response. It is thus evident that for a given M_W, the resulting correction ΔM_L is slightly larger for the Boatwright (1978) source spectrum than for the Brune (1970) source spectrum. For a given M_W, it is also slightly larger with the Wood-Anderson instrumental response included than with it omitted. Nonetheless, because the horizontal axis in Fig. 11 is 'true' magnitude, not 'uncorrected' magnitude, the corrections illustrated be applied directly. An iterative scheme was therefore devised, to indirectly determine the 'corrected' magnitude that corresponds to each reported 'uncorrected' magnitude.

The graphs in Fig. 11 indicate that magnitudes determined by GSK (2019) (and subsequently reported by Woo et al., 2019, and Langenbruch et al., 2019), specifically values of M_W determined in the time domain (after Tsuboi et al., 1995; Prejean and Ellsworth, 2001) and M_L values determined from amplitudes after synthesis of Wood-Anderson seismograms, can require significant correction. The size of this correction increases as M_W decreases and f_C increases, as f_C approaches, then exceeds, f_N. Conversely, the M_W values determined by Woo et al. (2019) in the frequency domain are evidently reliable, being comparable with other results (e.g., Grigoli et al., 2018; Kim Kwang- Hee et al., 2018). The 'Brune source, no instrument' graph in Fig. 11 can be used to

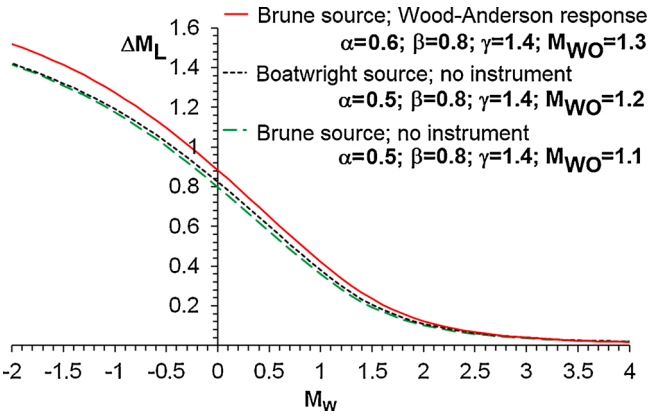

Fig. 11. Variation of the parameter ΔM_L, calculated using Eq. (25), with M_W, using Ψ determined using Eq. (24), with inputs stated representing different combinations of earthquake source models and instrumental response. Note the large size of this correction, ΔM_L, if M_W is very small.

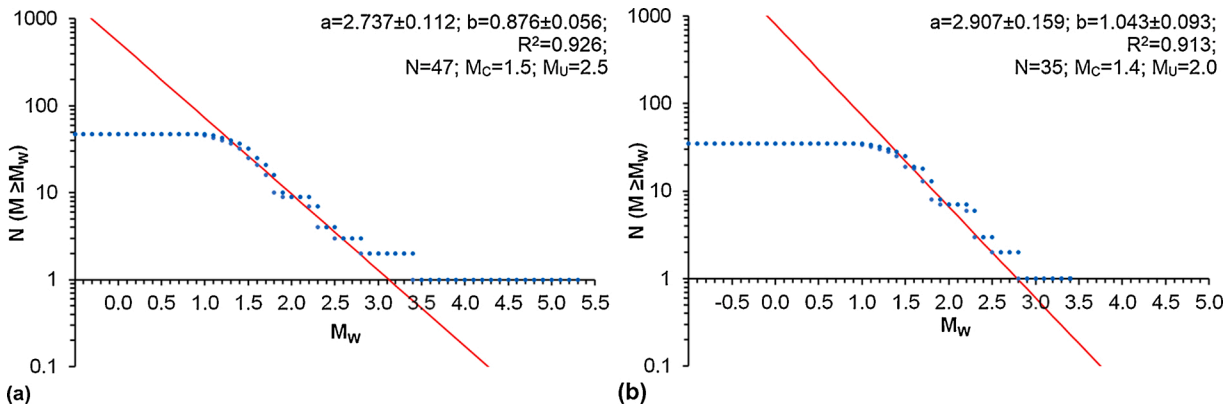

Fig. 12. Earthquake populations near the Pohang EGS site reported as M_W by GSK (2019), after correction for instrument bandwidth (see supplement 4). **(a)** Gutenberg-Richter law fit for the 47 events for which they determined M_W, following correction using the 'Brune source; no instrument' formula in Fig. 11. The effect of this correction can be seen by comparison with Fig. 9(b). **(b)** Gutenberg-Richter law fit for the events in common between the populations in part (a) and in Fig. 14 (a), following correction using the same procedure.

correct M_W values (Fig. 12(a)) and M_P values (Fig. 13), whereas the 'Brune source, Wood-Anderson response' graph can facilitate correction of M_L values. Strictly speaking, seismograms should of course be regarded as convolutions of source time functions with propagation effects, including the effect of anelastic attenuation, and with the instrumental response. The associated spectra are thus the products of the source spectrum U(f) with the effect of anelastic attenuation $1/P_S(f)$ from Eq. (8) and the spectrum of the instrumental response A(f). However, if Q_S is as high as is indicated by Kim et al. (2006) (Eq. (9)), then for the ~10 km distance to station PHA2 $P_S(f)$ does not depart significantly from 1 so anelastic attenuation has minimal effect. Nonetheless, the correction to M_L should be applied after consideration of its calibration, including use of station corrections (see below).

3.3. Correction for anelastic attenuation

Notwithstanding the high Q_S in the study area, an additional factor that might have influenced the M_L values determined by GSK (2019) is correction for anelastic attenuation, this being implicit in their use of the Sheen et al. (2018) procedure for determining M_L. In the time-domain calculations of M_W, the formula used by GSK (2019), after Prejean and Ellsworth (2001), corrects for geometrical spreading but not anelastic attenuation. However, the GSK (2019) determinations of M_L utilise a correction formula (after Sheen et al. (2018)) that attempts to combine the effects of both geometrical spreading and anelastic attenuation as the single parameter $A_O(R)$ (after Eq. (1)):

$$\log_{10}(A_O(R)) = -0.5107\ \log_{10}(R/100) - 0.001699\ (R - 100) - 3 \quad (26)$$

with hypocentral distance R in kilometres.

In Fig. 15, $A_O(R)$ from Eq. (26) is compared with direct calculations of effects of geometrical spreading and anelastic attenuation. For example, over R = 10–100 km, geometrical spreading of a single frequency component would cause ten-fold decrease in amplitude. However, this form of $A_O(R)$ predicts only a five-fold decrease in amplitude (i.e., a reduction in $\log_{10}(A_O)$ by ~0.7) over this distance range. This is much less than for other $A_O(R)$ calibrations, for example Miao and Langston (2007) reported

$$\log_{10}(A_O(R)) = -0.939\ \log_{10}(R/100) + 0.000276\ (R - 100) - 3 \quad (27)$$

for the central USA, a region of relatively high Q, whereas Hutton and Boore (1987) reported

$$\log_{10}(A_O(R)) = -1.110\ \log_{10}(R/100) - 0.00189\ (R - 100) - 3 \quad (28)$$

for southern California, a relatively low-Q region.

It thus appears probable that in this short-distance range (i.e., R < 100 km) the Sheen et al. (2018) A_O function is miscalibrated. The mismatch relative to the calculated curve for the expected anelastic attenuation at 40 Hz amounts in terms of magnitude units to ~0.3 at 50 km distance, ~0.8 at 10 km distance, ~0.9 at 6 km distance and ~1.1 at 3 km distance (Fig. 15). Given the form of Eq. (1), both this mismatch and the positive station corrections at nearby stations (the S values in Fig. 8), from the GSK (2019) analysis, will act to increase M_L values, when the issue on hand is underestimation. From the analyses already presented, two reasons are apparent for the systematic difference in S values between the temporary and permanent stations. The first factor is the underestimation of M_L caused by the low sampling interval of the

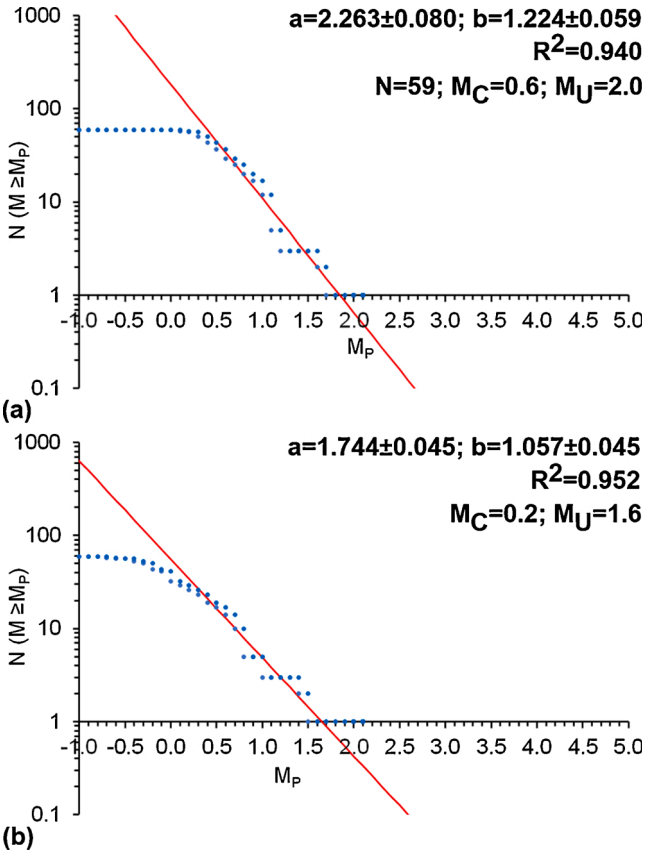

Fig. 13. **(a)** Earthquake population near the Pohang EGS site reported as M_P by GSK (2019), after correction for instrument bandwidth. **(b)** The corresponding population before correction, for comparison.

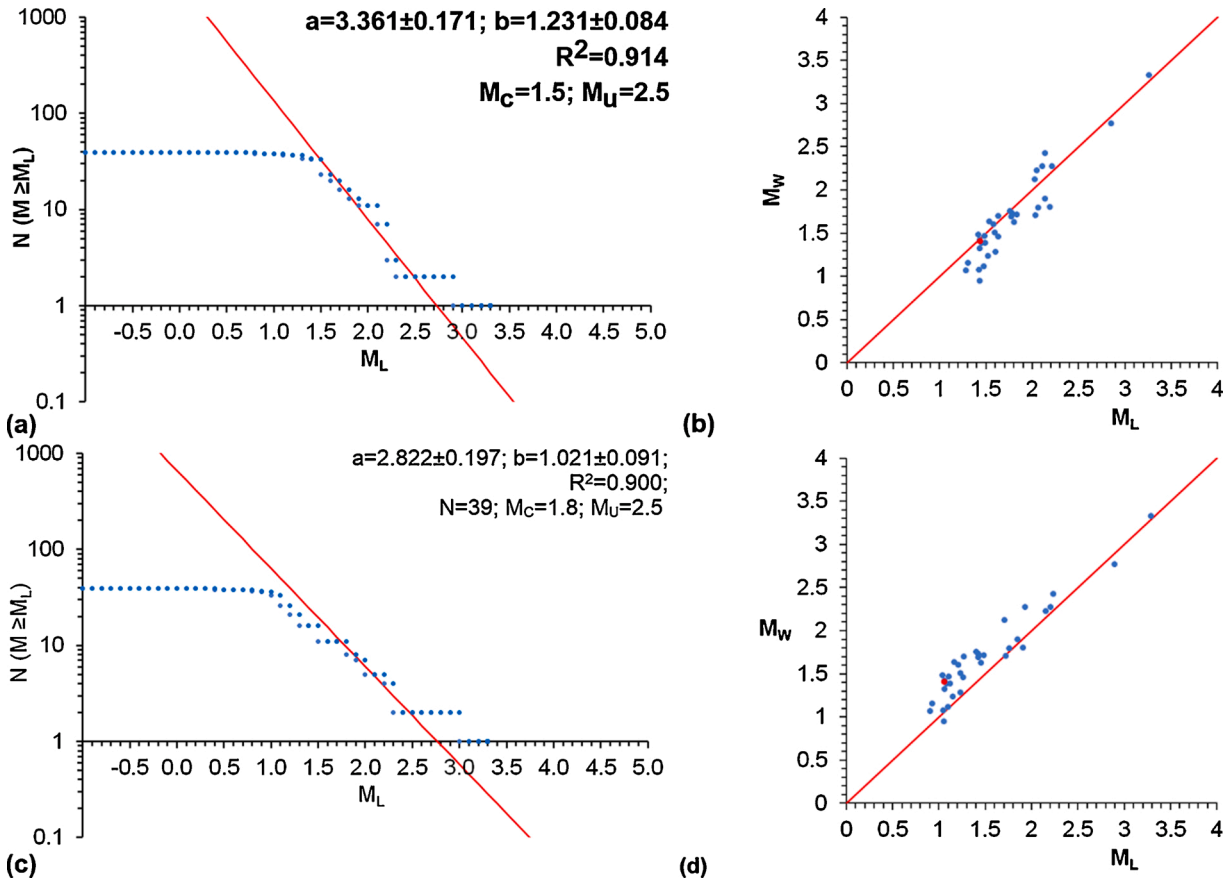

Fig. 14. **(a)** Gutenberg-Richter law fit for the 39 events for which GSK (2019) determined M_L values using synthetic Wood-Anderson seismograms, following correction using the 'Brune source; Wood-Anderson response' formula in Fig. 11, with $\delta M_L = 1.2$. The effect of this correction can be seen by comparison with Fig. 9 (c). **(b)** Scatter graph of M_W against M_L (from part (a), for $\delta M_L = 1.2$) for the 35 events in Fig. 12(b), with line for $M_W = M_L$, and highlighting of the event at 21:42 on 13 August 2017. **(c)** Same as (a), but for $\delta M_L = 0$. **(d)** Same as (b), but for $\delta M_L = 0$.

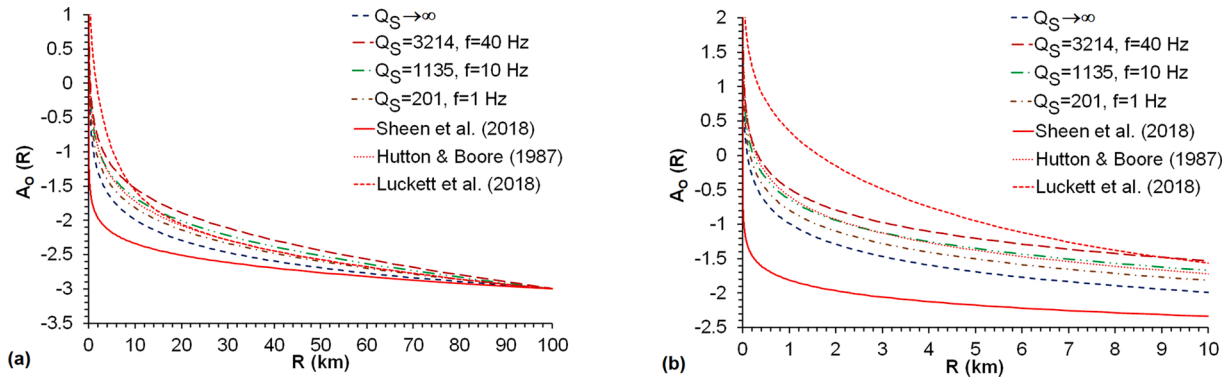

Fig. 15. Comparisons of the effects on the decrease of amplitude of seismic waves with source-station distance: after Eq. (5) of Sheen et al. (2018); for geometric spreading with no anelastic attenuation (i.e., for $Q_S \rightarrow \infty$); and (for $V_S = 3305$ m s^{-1}) for combinations of anelastic attenuation after Eq. (8) plus geometric spreading for frequency components with f = 1, 10 and 40 Hz, with $Q_S(f)$ after Kim et al. (2006) (Eq. (10)); and after Hutton and Boore (1987) and Luckett et al. (2019) . All variations are normalized with $\log_{10}(A_O) = -3$ at R = 100 km, consistent with Richter's (1935) definition of M_L. (a) For R = 0 to 100 km. (b) Enlargement for R = 0 to 10 km, showing the apparent non- physically realistic variations predicted by Sheen et al. (2018) and Luckett et al. (2019).

permanent stations (cf. Fig. 11), as already noted. The second factor, evident from Fig. 3, is the greater proximity of the temporary stations, resulting in greater overestimation of M_L given the form of the miscalibration of A_O by Sheen et al. (2018). The correction to GSK (2019) M_L values for miscalibration of the Sheen et al. (2018) A_O function will depend on the 'true' value of M_L, because this will determine the distance range over which each earthquake was recorded. Events of $M_L > \sim 2$ will be recorded across much of Korea, at many stations at R>>100 km, whose effect will outweigh that of the miscalibration of A_O at closer range and result in accurate values of M_L. On the other hand, for smaller events, recorded only by the temporary local network and/or station PHA2, this miscalibration and the positive station corrections at nearby stations are inferred to cause significant overestimation of M_L, partly offsetting the underestimation caused by the long sampling interval (see above). In summary, it would appear that for these smaller earthquakes, all three terms on the right-hand side of Eq. (1) are

systematically in error, the effects of these errors partly cancelling.

To begin to quantify these effects, it is recalled from Fig. 8 that the station corrections for the local seismograph network have an unweighted mean value of 0.598 ± 0.144 ($\pm 2s$), which is associated with a weighted mean value of 0.569 ± 0.154 (± 2 s). These stations were located ~3–6 km from the seismicity, at which distances the Sheen et al. (2018) calibration overestimates M_L by ~1.0. It follows after allowing for the station corrections that have been calculated or these stations, the M_L values for the earthquakes recorded by these stations should be increased by ~0.4. Furthermore, the data points in Fig. 8 that most likely correspond to station PHA2 indicate station corrections of ~0.4, but at ~10 km distance the Sheen et al. (2018) calibration overestimates M_L by ~0.8. More detailed evaluation is not possible here, because GSK (2019) did not report which of the station corrections in Fig. 8 applies to which station or which earthquakes were recorded by which stations. Nonetheless, it follows from these considerations that the correction to M_L to take account of the long sampling interval at station PHA2 should be applied to the 'raw' M_L values after subtraction of a correction δM_L, estimated as 1.2 magnitude units, to account for systematic errors in magnitude calibration. A workflow is thus devised to correct these magnitudes as reported by GSK (2019) and Woo et al. (2019). For $M_L < 2.0$, this involves subtracting $\delta M_L = 1.2$, then correction using Ψ calculated for the 'Brune source, Wood-Anderson response' graph in Fig. 11, then adding $\delta M_L = 1.2$ back on. Fig. 14(a) illustrates the result of this analysis; for comparison, Fig. 14(b) illustrates the result for $\delta M_L = 0$.

As is noted in supplement 1, GSK (2019) used the approximate 1:1 relation between their M_W and M_L values to validate both determinations; Woo et al. (2019) made the same argument. However, for the smaller events in this dataset, M_W typically exceeds M_L (Fig. 9(d)). The form of Fig. 11, with both types of magnitude diverging increasingly below their 'true' values as the earthquakes become smaller, M_L more so than M_W, explains this occurrence. This underestimation is clear for the 13 August 2017 events, as already noted. Gutenberg-Richter fits for the 'corrected' earthquake populations, for both M_W and M_L (Fig. 12 (a) and (b); Fig. 14 (a) and (c)), indicate b-values above (or just below) 1. Comparison of 'corrected' M_L and M_W values for individual earthquakes (Fig. 14 (b) and (d)) indicates that they are closer to equality: the tendency for M_W to exceed M_L, evident for the uncorrected data in Fig. 9(d), is still present, but has been significantly reduced, in Fig. 14(d), for $\delta M_L = 0$, whereas in Fig. 14(b), for $\delta M_L = 1.2$, there is a slight tendency for M_L to exceed M_W. These adjustments again reflect the corrections being larger for a given magnitude expressed as M_L than if expressed as M_W (Fig. 11). For the event at 21:42 on 13 August 2017, these correction procedures increase M_W from 1.205 to 1.409 and M_L from 0.67 to 1.06 (for $\delta M_L = 0$) or 1.44 (for $\delta M_L = 1.2$), bringing both much closer to the Hofmann et al. (2019) $M_W = 1.93$. Furthermore, since the correction for miscalibration of A_O will increase M_L more for smaller events than for larger ones, it will have the effect of 'compressing' the magnitude range of the earthquake population and thereby increasing its b-value, to 1.02 (Fig. 14(c), for $\delta M_L = 0$) or 1.23 (Fig. 14(a), for $\delta M_L = 1.2$), both values being close to the value 1.12 deduced from the Hofmann et al. (2019) analysis of the August 2017 stimulation of well PX-1. These considerations indicate that these correction procedures are on the right track, but because the corrected magnitudes do not correspond to $M_W = M_L$ and still underestimate the Hofmann et al. (2019) determination, the corrections that have been applied are insufficient. For example, if the true stress drop of the Pohang seismicity were higher than has been assumed, say ~10 MPa, the corner frequencies for each M_W would be higher (cf. Eq. (21)), which would result in smaller values of Ψ and thus larger corrections to magnitude (cf. Eq. (25)).

3.4. Correction of Langenbruch et al. (2020) template-matching magnitudes

As already noted, the magnitudes reported by Langenbruch et al. (2020) are a mix of M_L values from synthesis of Wood-Anderson seismograms, M_P values from use of empirical prediction equations, and M_T values from template-matching (see, also, supplement 4). The former subset of data consist of the same M_L values as were used by GSK (2019) and Woo et al. (2019) and so suffer from the same issues, relating to bandwidth limitation and the inconsistent definition of the Sheen et al. (2018) M_L formula. Their determination of M_T utilized Eq. (15), but with no clear basis for equating a ten-fold S-wave amplitude-ratio to one magnitude unit. As already noted, for the August 2017 earthquake population the ratio at station MSS01 was anyway ~20 (Fig. 6(b)) not 10. In terms of Eq. (17), a ratio of 20 means a template-matching scale factor $\Gamma = 1/\log_{10}(20) \approx 0.769$, so the Langenbruch et al. (2020) earthquake population would be 'compressed' into a smaller M_T range with a higher b-value. Thus, with $\Gamma = 1/\log_{10}(20) \approx 0.769$, the Gutenberg-Richter law fit in Fig. 4(a) adjusts to Fig. 16(a), with $b = 1.03 \pm 0.04$ and $M_C = 0.8$, whereas if $\Gamma = 0.64$ Fig. 4(a) adjusts to Fig. 16(b), with $b = 1.17 \pm 0.04$ and M_C again 0.8 (cf. Fig. 6(a)). However, as Langenbruch et al. (2020) did not state which template event, of which magnitude M_R, was used to determine M_T for which other events, the actual effect on the overall b-value of Γ being <1 cannot be established. Nonetheless, since correction for bandwidth limitation and for the template-matching scale factor can each, individually, increase b-values for this earthquake population to ~1, it is likely that combining each of the corrections would mimic the effect of lower Γ and result in b-values >1 (cf. Fig. 16(b)). The corrected values of M_W, M_L and M_T for this earthquake population, listed in supplement 4, show the separate corrections for individual events and provide a guide to the significance of these corrections in combination.

4. Discussion

The Pohang EGS project has been severely criticized, for example by Ellsworth et al. (2019), GSK (2019) and Langenbruch et al. (2020). This is not the place to review all aspects of the management of this project; only issues relevant to seismicity monitoring will be discussed. A first criticism is that the local monitoring network (Fig. 3(b)) was not in place early enough, dates of operation of individual stations being illustrated in Fig. S1 of Woo et al. (2019). Thus, although this network was installed in time for the first stimulation of well PX-2 in February 2016, it was not yet operational in November 2015 when the drilling of this well transected the Namsong Fault causing the aforementioned 'burst' of seismicity. As already noted, this seismicity went unrecognized until it was reported by Kim Kwang-Hee et al. (2018) following retrospective examination of archived data recorded at PHA2. The largest earthquake in this 'burst', at 03:52 on 30 November 2015, was reported by GSK (2019) with M_L 0.80 and M_W 0.97. Given the issues already noted, it probably adjusts to a 'true' magnitude somewhere between 1.5 and 2.0. Other jurisdictions have regulatory requirements for seismicity monitoring to be operational ahead of fluid injection; for example, in the UK it is required to start at least a year ahead. Had this been done at Pohang, the monitoring network would have 'caught' the November 2015 'burst' of seismicity and its implication, that the Namsong Fault had been 'breached' by the drilling and was critically stressed, would have been recognized and would undoubtedly have triggered a thorough review of the EGS project. Furthermore, it might have been anticipated ahead of any stimulation that knowledge of Q in the vicinity of the site would be important for magnitude calibration. Steps might thus have been taken to determine Q directly, for example using recordings of explosive shots of known strength at surface or borehole locations. Related issues concern the management of the local monitoring network and its data processing facility. There can be no satisfactory explanation for why the InSite software was not set up correctly until August 2017. As already noted, this resulted in the lack of M_W values for earthquakes before this time and created the requirement to develop a local M_I scale. Moreover, by August 2017 it was apparent that some stations of the local monitoring network had been unsuitably sited; some had not been maintained and had ceased to be operational. Other stations had been moved

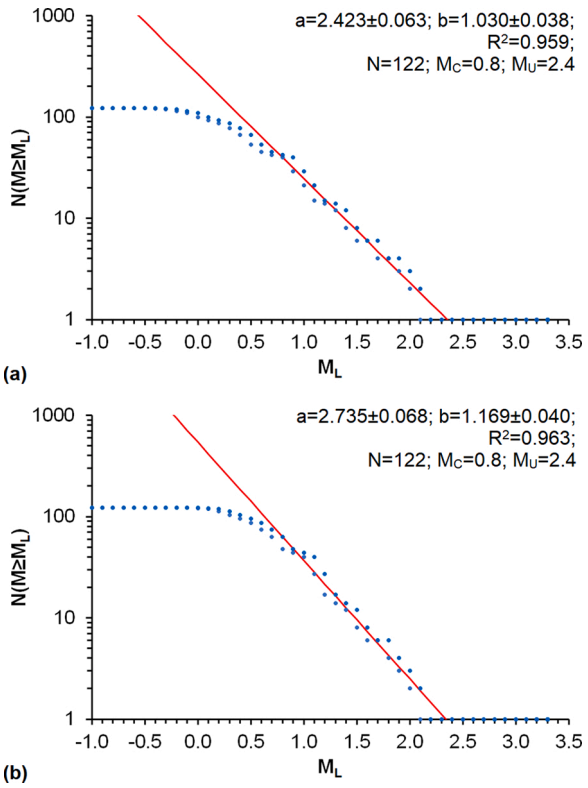

Fig. 16. Potential revisions to Fig. 4, suggesting possible corrected Gutenberg-Richter law fits for the 122 earthquakes reported by Langenbruch et al. (2020) (see supplement 4) from stimulations of well PX-2, using Eq. (18) for $M_R = 2.0$: **(a)** For $\Gamma = 1/\log_{10}(20) \approx 0.769$. **(b)** For $\Gamma = 0.64$.

to better sites (Fig. 3(b)) but retained the same names in their new locations; this is contrary to standard practice and created a potential source of error during retrospective analyses of the seismicity dataset. As will become clear below, the M_I scale that was ultimately developed provides an accurate proxy for 'true' magnitude values, such as M_W, but required significant extra workload that should have been unnecessary.

Arguably the most important management issue related to this seismicity monitoring concerns public engagement, meaning engagement not only with the population of Pohang but also with local officials and the Korean government. It is now evident (e.g., from Kim Kwang-Hee et al., 2018, and Rogers, 2018) that the earthquakes in the Pohang area, starting in early 2016, reported by KMA with $M_K \geq 2.0$, had attracted attention, especially given that the largest of these (at 02:31 on 15 April 2017; M_W 3.29; from stimulation of well PX-2) had been felt by local people. Associated concerns led to the award of funding to PNU for their own network of stations (illustrated in Figs. 2(a) and 3(b)), which became operational on 10 November 2017. This network was thus in position to record the transition from the tail of earthquakes associated with the September 2017 stimulation of well PX-2 to foreshocks, the 15 November mainshock, and aftershocks (e.g., Kim Kwang-Hee et al., 2018; GSK, 2019). However, despite such concerns, there is no record of any contact with the EGS developer, nor any record of the EGS developer reporting to the media or to any authority that their project was causing the sequence of earthquakes. Writing from the UK, a jurisdiction where such matters are highly regulated and subject to constant attention from the media and from environmental groups, these aspects are difficult to understand. There was, of course, no regulatory framework in Korea for anthropogenic seismicity at the time; as a result, as is detailed in multiple publications (e.g., Hofmann et al., 2018, 2019), the developer (in conjunction with research collaborators) was able to set their own 'traffic light scheme' thresholds.

The Korean Government Commission investigations into the Pohang EGS project have been praised by the media as the work of 'earthquake detectives', unravelling details that would otherwise have remained hidden (e.g., Baraniuk, 2019), even though most of the dataset analysed was provided on behalf of the developer in the first place. The Commission reports (Lee et al., 2019; GSK, 2019) and subsequent publications by Commission members (e.g., Ellsworth et al., 2019; Woo et al., 2019; Langenbruch et al., 2020; Yeo et al., 2020) indeed make many sound points. However, they have not engaged with the full dataset; notably absent is any consideration of groundwater chemistry, which appears key to understanding the coupling between chemical and mechanical processes within the Pohang granite (e.g., Westaway and Burnside, 2019; Westaway et al., 2020; Banks et al., 2021 this issue). Apart from reporting by GSK (2019) , the Commission also did not engage with the set of M_I values provided by the EGS developer (see supplement 4) and also did not appreciate the mismatch between their own magnitudes and those determined during the EGS project, notably for the August 2017 stimulation of well PX-1. The mismatch evident between the smallest earthquakes that could be identified during the EGS project, with M_C −0.2 (Hofmann et al., 2019; Fig. 6(a)), and the apparent much smaller events down to magnitude circa −1, reported by the Commission and the associated publications, with the Langenbruch et al. (2020) dataset seemingly indicating M_C −0.4 (Fig. 4), might also have been recognized. As already noted, Hofmann et al. (2019) located earthquakes recorded by the downhole geophone chain at R ~3 km, whereas the Commission outputs were based on data archived from permanent station PHA2, ~10 km away (Fig. 3(a)). Clearly, if it were possible to detect smaller earthquakes using permanent seismograph networks than can be achieved by installing dedicated instrumentation at site, the latter course of action would be pointless for EGS projects in general. It is unfortunate that Commission members, who include experienced earthquake seismologists, did not recognise these issues before placing their outputs, including the multiple publications, in the public domain.

Given their mismatches with the Commission outputs, the possibility has existed hitherto that it has been the magnitudes reported by EGS project participants (e.g., by Hofmann et al., 2019) that have been

inaccurate, rather than those determined by the Commission. If so, the basis of the August 2017 stimulation of well PX-1, the ability to determine accurate magnitudes in 'near real time' to implement the 'traffic light scheme', would be undermined. From the present investigation, it can now be concluded that the magnitudes determined to implement this 'traffic light scheme' were of sufficient accuracy for this purpose, thereby validating the approach taken for future reuse. Had Hofmann et al. (2019) included f_C for each earthquake, the robustness of these results would have been significantly strengthened; it is thus recommended that f_C be reported in future as routine when documenting earthquake populations from EGS projects, especially in cases where the significance of b-values might become an issue. Likewise, had the Commission reports and related publications been prepared with greater transparency, notably regarding which of the station corrections reported in Fig. 8 relate to which stations, and which earthquakes provided the 'templates' for matching which smaller events for determining M_T, it would have been possible to provide a fully quantitative set of corrections to their results rather than the part quantitative and part qualitative analysis that has been feasible.

It follows that the Commission did not recognize the potential impacts of the bandwidth limitation caused by the low sampling interval of permanent stations. An implication of the present study is that some of their outputs, such as earthquake magnitudes, are biased as a result of this limitation. This situation is similar to that in the 1980s during the transition from analog to digital seismometry. Researchers at that time (e.g., Hanks, 1982; Di Bona and Rovelli, 1988) deliberated on whether features they were analysing, at the limits of what might be recovered from the available data, were real features of earthquakes or artefacts of the digitization process. The use that has been made of data from PHA2 and other permanent stations clearly went beyond the purposes for which these data were recorded and might have been treated with similar caution. On the other hand, the high specification instruments at these stations might readily support much higher sampling intervals, say 1000 samples per second. However, interfacing of high-specification seismometers to digitizers operating at only 100 samples per second is quite engrained in the seismological community. In addition to its use in Japanese networks (e.g., Uchide and Imanishi, 2018) and in Korea, this sparse sampling interval is adopted as standard in the UK by BGS both for permanent network stations and for temporary deployments of local networks to monitor very small earthquakes caused by 'fracking' or mining (e.g., Luckett et al., 2019). Recording at 100 samples per second was also adopted during 2014–2016 for the NEONOR2 temporary network deployment in northern Norway, as well as for recording of the Central Italy earthquake sequence of 2017 (e.g., Chiaraluce et al., 2017; Janutyte et al., 2017; Luckett et al., 2019); the former project utilised digitizers that might have operated at 3000 samples per second (University of Bergen, 2015). The Southern California Seismic Network also records and archives most data with 100 samples per second, although some strong-motion records are sampled 200 times per second (Hauksson et al., 2020). Indeed, many publications do not report sampling intervals so this aspect cannot be checked. The rationale for recording at only 100 samples per second appears to be to limit the digital storage media needed. However, since digital storage capacity is inexpensive, there would seem to be no valid reason for continuing this practice. According to the manufacturer's data (Sercel, 2019a) the SlimWave downhole geophone chain used at Pohang could have operated at up to 1666 samples per second, rather than the 1000 samples per second adopted. However, this change would have only impacted on the ability to determine source parameters for earthquakes with M_W below circa −0.5 (Table 3), although no earthquakes as small as this have (yet) been identified in this dataset. Nonetheless, other geo-engineering projects have recorded at rates in excess of 10,000 samples per second (e.g., Collins and Young, 2000). This is not currently feasible for downhole instrumentation and is a technological limitation that prevents study of the source parameters of very small anthropogenic earthquakes.

The importance of this effect can be illustrated using a plot of amplitudes of P- and S-phases versus M_W, after Kwiatek and Ben-Zion (2016) (Fig. 17). The predicted amplitudes decrease with M_W, eventually falling below the background noise. Kwiatek and Ben-Zion (2016) estimated a background noise level of $\sim 5 \times 10^{-8}$ m s^{-1} from analysis of velocity power spectral density (PSD) for a worldwide ensemble of sites. Sheen et al. (2009) reported the acceleration PSD of the background noise for seismograph stations across Korea. Those in the Pohang area show values roughly consistent with the velocity PSD, and thus the noise amplitude, deduced by Kwiatek and Ben-Zion (2016). For comparison, other sites are noisier; for example, the U.S. site discussed by Takagishi et al. (2014) has a typical amplitude of cultural noise of $\sim 2 \times 10^{-7}$ m s^{-1}, thus with a higher earthquake detection threshold. The prediction graphs in Fig. 17 are from analyses by Kwiatek and Ben-Zion (2016) using parameter values as close as possible to those for the present study, such as $R = 10$ km and $V_R = 0.9\ V_S$, although with $\delta\sigma$ 1 or 10 MPa, rather than 5.6 MPa, and V_S 2887 rather than 3305 m s^{-1}, resulting in differences in derived parameters such as f_C as listed in Table 3. Moreover, the Kwiatek and Ben-Zion (2016) predictions are for a Trillium Compact sensor (Nanometrics Inc., Kanata, Ontario, Canada; Nanometrics, 2015) which, although similar in principle to the Güralp CMG-40T-1 sensor used at KMA station PHA2, has longer natural period of 120 s (supplement 2). Fig. 17 indicates that the spectral truncation of recording to $f_H = 40$ Hz at station PHA2, at $R = 10$ km, increases both the 'conventional' detection threshold (M_W), for a signal to noise (S/N) ratio of 5, from ~0.0 to ~0.4, and the 'template matching' detection threshold (M_W), for a S/N ratio of 0.1, from circa −1.2 to circa −0.4. The latter variation is in reasonable agreement with the present analysis where, for the smallest event detected by Langenbruch et al. (2020) (at 16:07 on 16 April 2017), M_T adjusts from −1.16 before correction (Fig. 4) to −0.43 after correction (Fig. 16(a)).

The Commission also did not recognize any limitation of the calibration of the Sheen et al. (2018) M_L scale, which (as already noted) has been widely used in their own outputs and related publications. This is perhaps not surprising, as the authors of this scale (Professor Tae-Seob Kang of Pukyong National University, Busan; Professor Dong- Hoon Sheen of Chonnam National University, Gwangju; and Dr Junkee Rhie of Seoul National University) were all Commission members. It is suggested that a new M_L calibration be devised for Korea and in the meantime the Sheen et al. (2018) scale should be assigned the warning 'not valid for $R < 100$ km'. The third problematic factor, the notion that a ten-fold ratio in amplitudes of seismograms equates to one magnitude unit (Langenbruch et al., 2020), or $F_T = 1.0$ in Eq. (15), forms the basis of

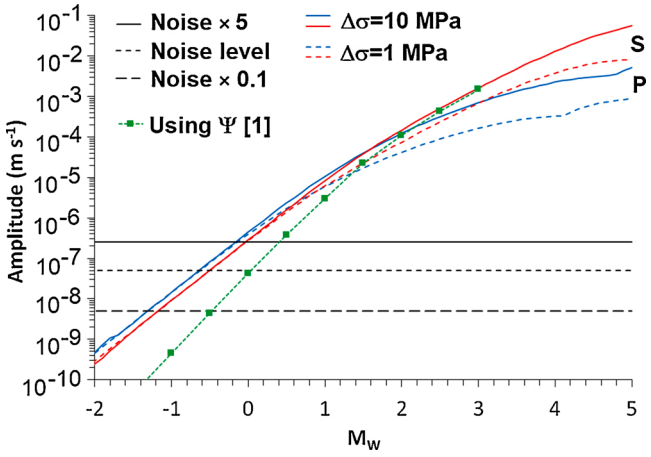

Fig. 17. Graph of predicted amplitude of seismic phases against M_W for $R = 10$ km and $V_R = 0.9\ V_S$, against background noise levels and detection thresholds, from Kwiatek and Ben-Zion (2016). Dotted line shows the modifications calculated in the present sudy using the variant [1] of the parameter Ψ in Table 3, for $f_H = 40$ Hz.

'template-matching' of magnitudes, but has no basis, beyond the special case of amplitudes for synthetic Wood- Anderson seismograms (cf., Richter, 1935). Nonetheless, the practice of doing this has become quite engrained, for example, it was used to determine some magnitudes in the Grigoli et al. (2018) study of Pohang. The present analysis is the first time that contradictions identified from using this approach have called its basis into question. In addition to the evidence in Fig. 6(b) for F_T ~1.24, Fig. 17 (after Kwiatek and Ben-Zion, 2016) also indicates that a unit difference in M_W (M_W −1.0 to 0.0) corresponds to an amplitude ratio of 30.7, indicating $F_T = \log_{10}(30.7) \approx 1.49$, or (after allowance for spectral truncation) 94.6, indicating F_T ~1.98, confirming that F_T should not automatically be assigned a value of 1. How this aspect is resolved, to enable continued use of 'template-matching' magnitudes, is an open question. One possibility is to adopt a new standard value for F_T, maybe ~1.25, after Fig. 6(b), or ~1.5, after Kwiatek and Ben-Zion (2016) (Fig. 17). It is also suggested that future 'template-matching' studies should report which template event was used to estimate the magnitudes of which other events, so their results can be simply corrected (using Eq. (15)) for a different value of F_T should this prove necessary. In the meantime, Bentz et al. (2020) have analysed the geomechanics of the Pohang site and made recommendations for the conduct of future EGS projects. However, their analysis is based on an inaccurate magnitude catalogue, from Ellsworth et al. (2019); it is thus invalid, but rectification is outside the scope of the present study. Online supplement 4 includes a catalogue of corrected magnitudes for Pohang earthquakes; its use will mitigate the consequences of future occurrences of this type.

A final consideration is the prediction of economic damage. It is well established that probabilities P of large-magnitude earthquakes can be predicted by extrapolation of the 'tails' of small-event populations (e.g., Smith, 1981). For this Pohang case study, Langenbruch et al. (2020) integrated such extrapolation with an economic model for probabilistic calculation of earthquake damage. By extrapolating the earthquake population from stimulation of well PX-2, these authors deduced that, ahead of the $M_W = 5.5$ earthquake, probabilities existed of ~5 % and ~1 %, respectively, for the occurrence of magnitude ≥5.0 and ≥6.0 events (Fig. 18(a)). Applying their economic model, Langenbruch et al. (2020) found that at the time of the Pohang mainshock, stimulation of well PX-2 had created a 1 % probability of causing damage costing US$3.2 billion, an order of magnitude more than the damage that actually occurred and two orders of magnitude greater than the value of the EGS project. Langenbruch et al. (2020) estimated that, as this project stood in November 2017, the combination of the ~2.3 % probability of occurrence of a magnitude 5.5 earthquake and the associated probable scale of economic losses was 'unacceptable'. Moreover, they concluded that, as early as the February 2016 PX-2 stimulation, the EGS developer might have identified a significant risk (e.g., P ~ 1.4 % for magnitude ≥5.0), even though the largest earthquake by then (at 22:04 on 7 February 2016) had been reported with

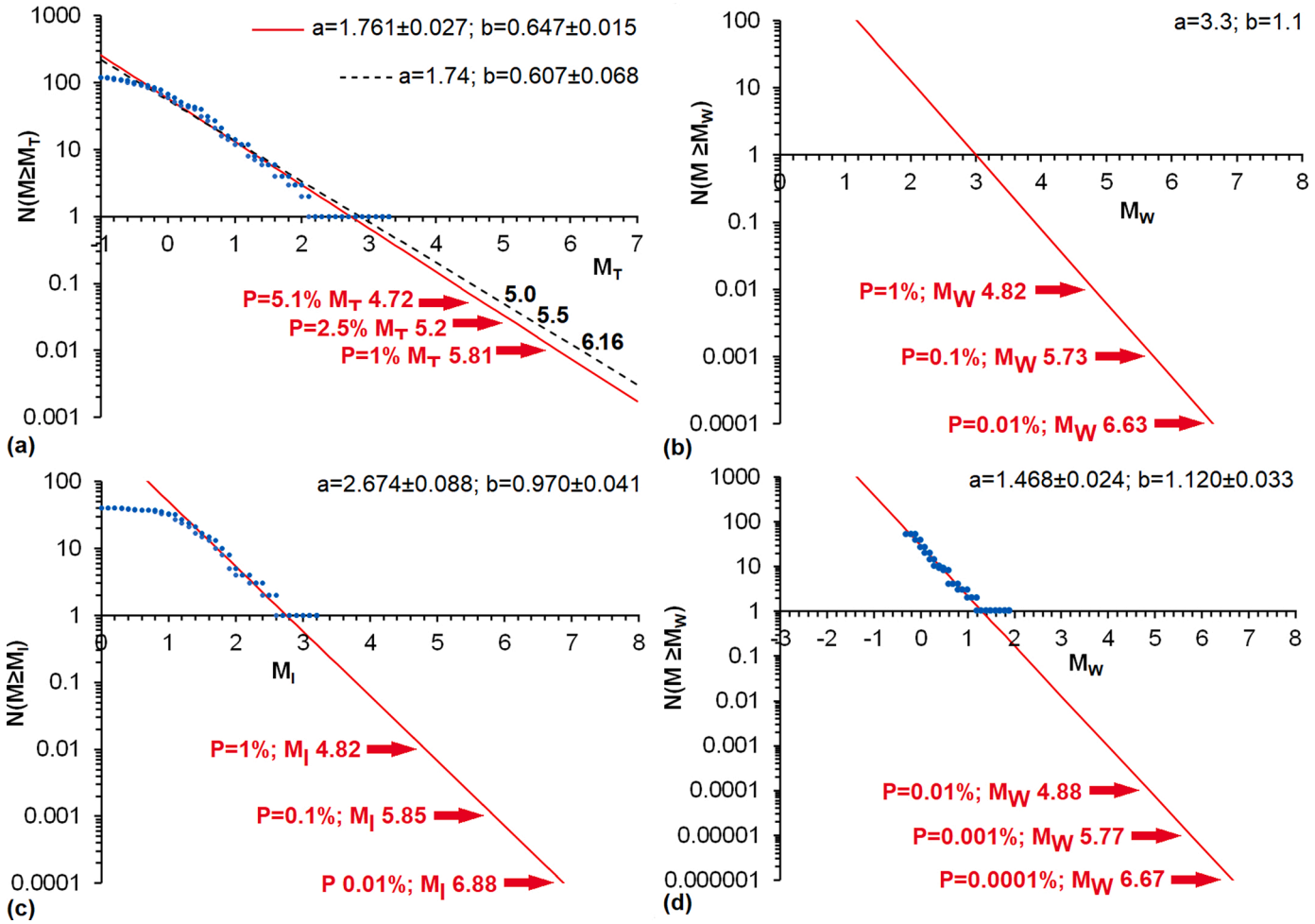

Fig. 18. Extrapolations of Gutenberg-Richter law fits for earthquake populations, showing associated representative probabilities of high-magnitude events. **(a)** For the earthquake population caused by stimulation of Pohang well PX-2, as reported by Langenbruch et al. (2020), with original and revised regression lines (after Fig. 4). **(b)** Suggested modification to the population in (a), after correction for the issues noted in the text and conversion to M_W. **(c)** For the earthquake population caused by stimulation of Pohang well PX-2, as reported to GSK (2019) by the EGS developer, from Fig. 7(b)). Note the similarity to the Gutenberg-Richter law fit proposed in (b). **(d)** For the earthquake population caused by the August 2017 stimulation of Pohang well PX-1, as reported by Hofmann et al. (2019) (Fig. 6(a)).

M_W only 1.62 and M_I only 1.67 (GSK, 2019). In the view of Langenbruch et al. (2020), at a 1% probability of occurrence the estimated damage already stood at US$10 million, rising to ~US$1 billion following the April 2017 stimulation, then to the aforementioned US$3.2 billion following the September 2017 stimulation. The implication of their analysis is that had these estimates been known to the developer, or to Korean regulators, the EGS project should have been terminated. However, this conclusion, and the underlying analysis, depend critically on the low b-value deduced for the earthquake population, and thus on the magnitudes on which it is based, having been accurately calibrated.

Taking into account each of the three identified issues that have caused underestimation of magnitudes reported by Langenbruch et al. (2020) and associated b-values, in accordance with previous discussion, it is suggested that when in the range ~2–3 their magnitudes are more-or-less correct, but for the events reported circa magnitude −1 the 'true' magnitudes are circa $M_W + 1$. The associated b- values adjust to values in excess of 1, circa 1.1, and, as shown in Fig. 18(b), the probability of an event of M_W circa 6.2 is reduced by a factor of ~30, from the ~1% of Langenbruch et al. (2020) to ~0.03 %. Using their economic analysis, with this revised earthquake population, a ~1% probability of occurrence would correspond to M_W ~4.8 and would have estimated economic costs of ~US$0.5 million. It would thus still be significant, but would only represent a small proportion of the value of the project and should be readily coverable by insurance. These considerations highlight the need for an agreed framework for specifying the economic risk from EGS projects and how these are covered. Estimation of notional economic 'risks' based on extrapolation of Gutenberg-Richter law fits to earthquake populations (cf. Langenbruch et al., 2020) itself requires an agreed specification to ensure accuracy of earthquake magnitudes and associated b-values.

Fig. 18(c) shows an extrapolation of the population of M_I values reported by the EGS developer to GSK (2019) for earthquakes associated with PX-2 stimulations. It is strikingly similar in form to Fig. 18(b), suggesting that these M_I values are accurate proxies for standard magnitude determinations, M_W or 'true' M_L. There is no basis from this dataset for any significant expectation of any earthquake as large as M_W 5.5 and thus no reason on the basis of this seismicity why the developer might have considered suspending the EGS project ahead of the November 2017 mainshock. The criticism of the EGS developer over this aspect, stated most strongly by Ellsworth et al. (2019) and Langenbruch et al. (2020) and in a more muted form by GSK (2019), is thus unfair. Moreover, the greater accuracy of the set of magnitudes determined by the EGS developer, relative to those determined subsequently by the Commission, deserves recognition.

Fig. 18(d) shows an extrapolation of the population of M_W values reported by Hofmann et al. (2019) for earthquakes associated with the August 2017 stimulation of well PX-1. The resulting probabilities of occurrence of each magnitude of large earthquake, and the associated costs of damage, are roughly two orders-of-magnitude below those for the PX-2 populations assessed in Fig. 18(b) and (c). The wisdom of the 'soft stimulation' technique adopted in August 2017 (Hofmann et al., 2018, 2019) is thus well demonstrated, in lieu of what might be termed the more 'heavy handed' approach, involving wellhead pressures up to ~90 MPa (e.g., Park et al., 2017), adopted during the December 2016 stimulation of well PX-1 and the three stimulations of well PX-2. However, this does not mean that this August 2017 stimulation played no part in creating the conditions for the occurrence of the November 2017 mainshock; as has been previously reported (e.g., Westaway and Burnside, 2019; Westaway et al., 2020) this stimulation involved injection of surface water followed by production of a roughly equal volume of water that was mostly original in situ groundwater, not the injected surface water. The injected surface water that remained in the Pohang granite was not in chemical equilibrium with its surroundings and will have dissolved minerals along the faults and fractures within which it remained. As Westaway and Burnside (2019) showed, this process will have altered the local state of stress towards the Coulomb condition for slip; however, it is unknown whether any of this injected surface water remained within the Namsong Fault, rather than within other faults and fractures within the Pohang granite. Research into this aspect continues; it highlights the point that the probability of occurrence of a large earthquake as a result of an EGS project in granite is not simply a matter of Gutenberg-Richter law extrapolation.

5. Conclusions

The M_W 5.5 Pohang earthquake on 15 November 2017, caused by the Pohang EGS project, caused one fatality and ~US$300 million of economic consequences. The Korean Government Commission to investigate this earthquake has released data including magnitudes of the populations of smaller earthquakes associated with the well stimulations. On the basis of these earthquake populations, it has been proposed that a significant probability of such losses was predictable beforehand, and that the project should have been suspended, implying that its developer was remiss for not doing so. This argument depends on the low estimated b-value, ~0.61, of this earthquake population. The main aim of the present study has been to shed light on the reasons for the significant mismatches between the earthquake magnitudes determined by participants in the Pohang EGS project (e.g., by Hofmann et al. (2019)), and those reported by the Commission (Lee et al., 2019; GSK, 2019) and used in subsequent publications. The magnitude datasets derived from the Commission activities have been shown to suffer from three significant sources of systematic error. These sources, which affect different types of magnitude determination differently, arise from the limited bandwidth of digital recording by the permanent seismograph stations, from miscalibration of the Sheen et al. (2018) formula used in Korea for determining M_L scale, and from miscalibration of the relation used to estimate magnitudes of smaller events from larger events by template matching. These factors all cause underestimation of magnitudes of the smallest events documented, resulting in underestimation of b- values. The true b-values are higher, being 1.12 for the August 2017 stimulation of well PX-1, for which magnitudes were accurately measured by Hofmann et al. (2019); similar values are estimated for the other well stimulations. A consequence of this analysis is that the probability of any earthquake as large as $M_W = 5.5$, predicted ahead of its occurrence by extrapolation using observed b-values, was much lower than has been claimed. This analysis highlights the need for agreed specifications, first, for acceptable economic risk arising from EGS projects and, second, for reporting seismicity datasets (such as that in the present study), especially where these might influence prosecutions of EGS developers.

Data availability

Data presented in this paper are publicly available from download links provided by the cited references. An integrated compilation of these data, for earthquake source parameters, is provided as part of the present online supplement.

CRediT authorship contribution statement

Rob Westaway: Conceptualization, Methodology, Validation, Formal analysis, Investigation, Data curation, Writing - original draft, Writing - review & editing, Visualization.

Declaration of Competing Interest

The author declares that he has no competing financial interests or personal relationships that could have appeared to influence the work reported in this paper.

Acknowledgments

This work was supported by the European Commission Horizon 2020 research and innovation programme under grant agreement No. 691728 (DESTRESS). Martin Mai and an anonymous reviwer are thanked for their thoughtful and constructive comments.

Appendix A. Supplementary data

Supplementary data associated with this article can be found, in the online version, at https://doi.org/10.1016/j.geothermics.2020.102035.

References

Ahern, T.K., Dost, B., 2006. SEED Reference Manual: Standard for the Exchange of Earthquake Data, v. 2.4. Incorporated Research Institutions for Seismology, Seattle, Washington, p. 224. http://www.fdsn.org/pdf/SEEDManual_V2.4.pdf.

Albaric, J., Oye, V., Langet, N., Hasting, M., Lecomte, I., Iranpour, K., Messeiller, M., Reid, P., 2014. Monitoring of induced seismicity during the first geothermal reservoir stimulation at Paralana, Australia. Geothermics 52, 120–131.

Amato, A., Mele, F.M., 2007. Performance of the INGV national seismic network from 1997 to 2007. Anal. Geophys. 51, 417–431.

Bachmann, C.E., Wiemer, S., Goertz-Allmann, B.P., Woessner, J., 2012. Influence of pore-pressure on the event-size distribution of induced earthquakes. Geophys. Res. Lett. 39, L09302 https://doi.org/10.1029/2012GL051480.

Baisch, S., Vörös, R., Weidler, R., Wyborn, D., 2009. Investigation of fault mechanisms during geothermal reservoir stimulation experiments in the Cooper Basin, Australia. Bull. Seismol. Soc. Am. 99, 148–158.

Banks, D., Boyce, A., Westaway, R., Burnside, N.M., 2021. Sulphur isotopes in deep groundwater reservoirs: evidence from post-stimulation flowback at the Pohang geothermal facility, Korea. Geothermics this issue.

Baraniuk, C., 2019. The mystery of unexplained earthquakes: from the UK to South Korea, seismic "detectives" are tracking the causes of anomalous tremors. BBC Future online. https://www.bbc.com/future/article/20190708-the-mystery-of-unexplained-earthquakes.

Bentz, S., Kwiatek, G., Martínez-Garzón, P., Bohnhoff, M., Dresen, G., 2020. Seismic moment evolution during hydraulic stimulations. Geophys. Res. Lett. 47, 9. https://doi.org/10.1029/2019GL086185 e2019GL086185.

Boatwright, J., 1978. Detailed spectral analysis of two small New York State earthquakes. Bull. Seismol. Soc. Am. 68, 1117–1131.

Boatwright, J., 1980. A spectral theor for circular seismic sources: simple estimates of source dimension, dynamic stress drop and radiated energy. Bull. Seismol. Soc. Am. 70, 1–27.

Boese, C.M., Wotherspoon, L., Alvarez, M., Malin, P., 2015. Analysis of anthropogenic and natural noise from multilevel borehole seismometers in an urban environment, Auckland, New Zealand. Bull. Seismol. Soc. Am. 105, 285–299. https://doi.org/10.1785/0120130288.

Boore, D.M., 1983. Stochastic simulation of high-frequency ground motions based on seismological models of the radiated spectra. Bull. Seismol. Soc. Am. 73, 1865–1894.

Boore, D.M., Boatwright, J., 1984. Average body-wave radiation coefficients. Bull. Seismol. Soc. Am. 74, 1615–1621.

Bromley, C.J., Pearson, C.F., Rigor Jr., D.M., PNOC-EDC, 1987. Microearthquakes at the Puhagan geothermal field, Philippines—a case of induced seismicity. J. Volcanol. Geotherm. Res. 31, 293–311.

Brune, J., 1970. Tectonic stress and the spectra of seismic shear waves from earthquakes. J. Geophys. Res. 75, 4997–5009 (with 1971 correction: Journal of Geophysical Research, 76, 5002.

Butcher, A., Luckett, R., Verdon, J., Kendall, M., Baptie, B., Wookey, J., 2017. Local magnitude discrepancies for near-event receivers: implications for the UK traffic-light scheme. Bull. Seismol. Soc. Am. 107, 532–541. https://doi.org/10.1785/0120160225.

Chiaraluce, L., Di Stefano, R., Tinti, E., Scognamiglio, L., Michele, M., Casarotti, E., Cattaneo, M., De Gori, P., Chiarabba, C., Monachesi, G., Lombardi, A., Valoroso, L., Latorre, D., Marzorati, S., 2017. The 2016 Central Italy seismic sequence: a first look at the mainshocks, aftershocks, and source models. Seismol. Res. Lett. 88, 757–771. https://doi.org/10.1785/0220160221.

Collins, D.S., Young, R.P., 2000. Lithological controls on seismicity in granitic rocks. Bull. Seismol. Soc. Am. 90, 709–723.

D'Amico, M., Puglia, R., Russo, E., Maini, C., Pacor, F., Luzi, L., 2017. SYNTHESIS: a web repository of synthetic waveforms. Bull. Earthq. Eng. 15, 2483–2496. https://doi.org/10.1007/s10518-016-9982-8.

Deichmann, N., 2006. Local magnitude, a moment revisited. Bull. Seismol. Soc. Am. 96, 1267–1277.

Dempsey, D., Suckale, J., Huang, Y., 2016. Collective properties of injection-induced earthquake sequences: 2. Spatiotemporal evolution and magnitude frequency distributions. J. Geophys. Res. Solid Earth 121, 3638–3665.

Di Bona, M., Rovelli, A., 1988. Effects of the bandwidth limitation on stress drops estimated from integrals of the ground motion. Bull. Seismol. Soc. Am. 78, 1818–1825.

Dorbath, L., Cuenot, N., Genter, A., Frogneux, M., 2009. Seismic response of the fractured and faulted granite of Soultz-sous-Forêts (France) to 5 km deep massive water injections. Geophys. J. Int. 177, 653–675.

Ellsworth, W.L., Giardini, D., Townend, J., Ge, S.M., Shimamoto, T., 2019. Triggering of the Pohang, Korea, earthquake (M_w 5.5) by Enhanced Geothermal System stimulation. Seismol. Res. Lett. 90, 1844–1858.

Eshelby, J.D., 1957. The determination of the elastic field of an ellipsoidal inclusion, and related problems. Proc. R. Soc. Lond. Ser. A 241, 376–396.

Frankel, A., 2009. A constant stress-drop model for producing broadband synthetic seismograms: comparison with the Next Generation Attenuation relations. Bull. Seismol. Soc. Am. 99, 664–680.

Grigoli, F., Cesca, S., Rinaldi, A.P., Manconi, A., López-Comino, J.A., Clinton, J.F., Westaway, R., Cauzzi, C., Dahm, T., Wiemer, S., 2018. The November 2017 M_w 5.5 Pohang earthquake: a possible case of induced seismicity in South Korea. Science 360, 1003–1006.

GSK, 2019. Final Report of the Korean Government Commission on Relations Between the 2017 Pohang Earthquake and EGS Project. The Geological Society of Korea, Seoul, p. 427. https://doi.org/10.22719/KETEP-2019043001 (in Korean).

Güralp, 2006. CMG-40T-1 Triaxial Broadband Seismometer. Operator's Guide. Güralp Systems Ltd., Aldermaston, England, p. 33. https://www.guralp.com/documents/MAN-040-0002.pdf.

Gutro, R., 2017. Noru (Northwest Pacific). NASA Goddard Space Flight Center, Greenbelt, Maryland, USA. https://www.nasa.gov/feature/goddard/2017/noru-northwest-pacific.

Hanks, T.C., 1982. F_{max}. Bull. Seismol. Soc. Am. 72, 1867–1879.

Hanks, T.C., Kanamori, H., 1979. A moment magnitude scale. J. Geophys. Res. 84, 2348–2350.

Hauksson, E., Yoon, C., Yu, E., Andrews, J.R., Alvarez, M., Bhadha, R., Thomas, V., 2020. Caltech/USGS southern California seismic network (SCSN) and southern California earthquake data center (SCEDC): data availability for the 2019 Ridgecrest sequence. Seismol. Res. Lett. 91, 1961–1970.

Hofmann, H., Zimmermann, G., Zang, A., Min, K.-B., 2018. Cyclic soft stimulation (CSS): a new fluid injection protocol and traffic light system to mitigate seismic risks of hydraulic stimulation treatments. Geotherm. Energy 6 (1). https://doi.org/10.1186/s40517-018-0114-3.

Hofmann, H., Zimmermann, G., Farkas, M., Huenges, E., Zang, A., Leonhardt, M., Kwiatek, G., Martinez-Garzon, P., Bohnhoff, M., Min, K.-B., Fokker, P., Westaway, R., Bethmann, F., Meier, P., Yoon, K.S., Choi, J.W., Lee, T.J., Kim, K.Y., 2019. First field application of cyclic soft stimulation at the Pohang enhanced Geothermal System site in Korea. Geophys. J. Int. 217, 926–949.

Hutton, L.K., Boore, D.M., 1987. The M_L scale in southern California. Bull. Seismol. Soc. Am. 77, 2074–2094.

IRIS PASSCAL, 2020. Guralp CMG-40T-1 Short Period Sensor. IRIS PASSCAL Instrument Center, Socorro, New Mexico. https://www.passcal.nmt.edu/content/instrumentation/sensors/short-period-sensors/cmg-40t-1-sp- sensor.

Itasca, 2019. InSite Seismic Processor: Technical Appendix, January 17, 2019, v 3.15. Itasca Consulting Ltd., Shrewsbury, England, p. 116. https://itasca-software.s3.amazonaws.com/resources/InSiteAppendices.pdf.

Janutyte, I., Lindholm, C., Olesen, O., 2017. Relation between seismicity and tectonic structures offshore and onshore Nordland, northern Norway. Nor. J. Geol. 97, 211–225. https://doi.org/10.17850/njg97-3-02.

Kagan, Y.Y., 2002. Seismic moment distribution revisited: I. Statistical results. Geophys. J. Int. 148, 520–541.

Kaneko, Y., Shearer, P.M., 2014. Seismic source spectra and estimated stress drop derived from cohesive-zone models of circular subshear rupture. Geophys. J. Int. 197, 1002–1015.

Kim, S.K., Park, M.A., 2002. The local magnitude scale in the Korean Peninsula. J. Geol. Soc. Korea 38, 217–235 (in Korean with English abstract).

Kim, S.K., Yang, J.Y., Oh, J., 2006. Q-values for P and S waves in the southern Korean Peninsula based on the coda-normalization method. Geosci. J. 10, 465–477.

Kim Kwang-Hee, Ree, J.-H., Kim, Y., Kim, S., Kang, S.Y., Seo, W., 2018. Assessing whether the 2017 M_w 5.4 Pohang earthquake in South Korea was an induced event. Science 360, 1007–1009.

Kim Kwang-Il, Min, K.-B., Kim, K.-Y., Choi, J.W., Yoon, K.-S., Yoon, W.S., Yoon, B.J., Lee, T.J., Song, Y.H., 2018. Protocol for induced microseismicity in the first enhanced geothermal systems project in Pohang, Korea. Renew. Sust. Energy Rev. 91, 1182–1191.

Kinemetrics, 2017. EpiSensor force balance accelerometer. Kinemetrics, Inc., Pasadena, California, p. 2. https://kinemetrics.com/wp- content/uploads/2017/04/data sheet-episensor-es-t-force-balance-accelerometer-kinemetrics.pdf.

Kinemetrics, 2019. Quanterra Q330S Very Low-power High-resolution Integrated Seismic System. Kinemetrics, Inc., Pasadena, California, p. 2. https://kinemetrics.com/wp-content/uploads/2019/11/Q330S-Datasheet.pdf.

KMA, 2019. Korea Seismic Observation Network. Korea Meteorological Administration, Seoul. http://web.kma.go.kr/eng/weather/kma_service/observation.jsp.

Kwiatek, G., Ben-Zion, Y., 2016. Theoretical limits on the detection and analysis of small earthquakes. J. Geophys. Res. Solid Earth 121, 5898–5916. https://doi.org/10.1002/2016JB012908.

Kwiatek, G., Saarno, T., Ader, T., Bluemle, F., Bohnhoff, M., Chendorain, M., Dresen, G., Heikkinen, P., Kukkonen, I., Leary, P., Leonhardt, M., Malin, P., Martínez-Garzón, P., Passmore, K., Passmore, P., Valenzuela, S., Wollin, C., 2019. Controlling fluid-induced seismicity during a 6.1-km-deep geothermal stimulation in Finland. Sci. Adv. 5, 12. https://doi.org/10.1126/sciadv.aav7224 eaav7224.

Langenbruch, C., Ellsworth, W.L., Woo, J.-U., Wald, D.J., 2020. Value at induced risk: injection-induced seismic risk from low-probability, high-impact events. Geophys. Res. Lett. 47, 12. https://doi.org/10.1029/2019GL085878 e2019GL085878.

Leary, P., Malin, P., Saarno, T., 2020. A physical basis for gutenberg-richter fractal scaling. In: Proceedings, 45th Workshop on Geothermal Reservoir Engineering. Stanford University, Stanford, California, 10–12 February 2020, Paper SGP-TR-216,

p. 11. https://pangea.stanford.edu/ERE/db/GeoConf/papers/SGW/2020/Leary1.pdf.
Lecocq, T., Hicks, S.P., Van Noten, K., Kasper van Wijk, K., Koelemeijer, P., De Plaen, R.S. M., Massin, F., Hillers, G., Anthony, R.E., Apoloner, M.-T., Arroyo- Solórzano, M., Assink, J.D., Büyükakpınar, P., Cannata, A., Cannavo, F., Carrasco, S., Caudron, C., Chaves, E.J., Cornwell, D.G., Craig, D., den Ouden, O.F.C., Diaz, J., Donner, S., Evangelidis, C.P., Evers, L., Fauville, B., Fernandez, G.A., Giannopoulos, D., Gibbons, S.J., Girona, T., Grecu, B., Grunberg, M., Hetényi, G., Horleston, A., Inza, A., Irving, J.C.E., Jamalreyhani, M., Kafka, A., Koymans, M.R., Labedz, C.R., Larose, E., Lindsey, N.J., McKinnon, N., Megies, T., Miller, M.S., Minarik, W., Moresi, L., Márquez-Ramírez, V.H., Möllhoff, M., Nesbitt, I.M., Niyogi, S., Ojeda, J., Oth, A., Proud, S., Pulli, J., Retailleau, L., Rintamäki, A.E., Satriano, C., Savage, M. K., Shani- Kadmiel, S., Sleeman, R., Sokos, E., Stammler, K., Stott, A.E., Subedi, S., Sørensen, M.B., Taira, T., Tapia, M., Turhan, F., van der Pluijm, B., Vanstone, M., Vergne, J., Vuorinen, T.A.T., Warren, T., Wassermann, J., Xiao, H., 2020. Global quieting of high-frequency seismic noise due to COVID- 19 pandemic lockdown measures. Science 369, 1338–1343.
Lee, W.H.K., Bennet, R.E., Meaghu, K.L., 1972. A method of estimating magnitude of local earthquakes from signal duration. U.S. Geological Survey Open File Report 1972-223, p. 28.
Lee, T.J., Song, Y.H., Yoon, W.S., Kim, K.-Y., Jeon, J.G., Min, K.-B., Cho, Y.-H., 2011. The first enhanced geothermal system project in Korea. In: Proceedings of the 9th Asian Geothermal Symposium. November 7–9, 2011. https://www.geothermal-energy.org/pdf/IGAstandard/Asian/2011/23_Tae_Jong_Lee.pdf.
Lee, K.-K., Yeo, I.-W., Lee, J.-Y., Kang, T.-S., Rhie, J., Sheen, D.-H., Chang, C., Son, M., Cho, I.-K., Oh, S., Pyun, S., Kim, S., Ge, S., Ellsworth, W.L., Giardini, D., Townend, J., Shimamoto, T., 2019. Summary Report of the Korean Government Commission on Relations Between the 2017 Pohang Earthquake and the EGS Project. Geological Society of Korea and Korean Government Commission on the Cause of the Pohang Earthquake, Seoul, Republic of Korea, p. 205. http://www.gskorea.or.kr/custom/27/data/Summary_Report_on_Pohang_Earthquake_March_20_2019.pdf.
Longuet-Higgins, M.S., 1950. A theory of the origin of microseisms. Philos. Trans. R. Soc. Lond. A 243, 1–35.
Luckett, R., Ottemöller, L., Butcher, A., Baptie, B., 2019. Extending local magnitude M_L to short distances. Geophys. J. Int. 216, 1145–1156.
Madariaga, R., 1976. Dynamics of an expanding circular fault. Bull. Seismol. Soc. Am. 66, 639–666.
Madariaga, R., Ruiz, S., 2016. Earthquake dynamics on circular faults: a review 1970–2015. J. Seismol. 20, 1235–1252.
Mandal, P., Narasaiah, R., Raju, P.S., Chandha, R.K., 2004. Coda duration magnitude scale of 2001 Bhuj aftershoks, India. Curr. Sci. 87, 520–527.
Miao, Qing Wen, Langston, C.A., 2007. Empirical distance attenuation and the local-magnitude scale for the Central United States. Bull. Seismol. Soc. Am. 97, 2137–2151.
Nanometrics, 2015. Trillium Compact: User Guide. Nanometrics Inc., Kanata, Ontario, Canada, p. 75. https://www-iuem.univ- brest.fr/pops/attachments/download/1489/trilliumcompact_userguide.pdf.
Ottemöller, L., Sargeant, S., 2013. A local magnitude scale M_L for the United Kingdom. Bull. Seismol. Soc. Am. 103, 2884–2893.
Park, S., Xie, L., Kim, K.-I., Kwon, S., Min, K.-B., Choi, J., Yoon, W.-S., Song, Y., 2017. First hydraulic stimulation in fractured geothermal reservoir in Pohang PX-2 well. Procedia Eng. 191, 829–837.
Parsons, T., Geist, E.L., Console, R., Carluccio, R., 2018. Characteristic earthquake magnitude frequency distributions on faults calculated from consensus data in California. J. Geophys. Res. Solid Earth 123, 10,761–10,784. https://doi.org/10.1029/2018JB016539.
Peng, Z.G., Zhao, P., 2009. Migration of early aftershocks following the 2004 Parkfield earthquake. Nat. Geosci. 2, 877–881.
Prejean, S.G., Ellsworth, W.L., 2001. Observations of earthquake source parameters at 2 km depth in the Long Valley Caldera, Eastern California. Bull. Seismol. Soc. Am. 91, 165–177.
Quanterra, 2007. Q330 Operations Guide: Q330HR/Q330 Operation, Overview of Support Tools. Baler Operation Quanterra, Inc., Harvard, Massachusetts, p. 318. http://epsc.wustl.edu/~patrick/load/Quanterra-Q330-docs/304808B-Q330-OperationsGuide.pdf.
Richter, C.F., 1935. An instrumental earthquake magnitude scale. Bull. Seismol. Soc. Am. 25, 1–32.
Rogers, N., 2018. Damaging earthquake in South Korea last year may have been caused by geothermal fracking. Inside Sci. 26 April 2018 https://www.insidescience.org/news/damaging- earthquake-south-korea-last-year-may-have-been-caused-geothermal-fracking.
Sato, T., Hirasawa, T., 1973. Body wave spectra from propagating shear cracks. J. Phys. Earth 21, 415–431.
Sercel. Downhole specifications. Sercel, Nantes, France. https://www.sercel.com/products/Lists/ProductSpecification/Downhole_Specifications_Sercel_EN.pdf 2019;.
Sercel. Geophones specifications. Sercel, Nantes, France. https://www.sercel.com/products/Lists/ProductSpecification/Geophones_specifications_Sercel_EN.pdf 2019;.
Sheen, D.-H., 2015. Comparison of local magnitude scales in South Korea. J. Geol. Soc. Korea 51, 415–424 (in Korean with English abstract).
Sheen, D.-H., Shin, J.S., Kang, T.-S., 2009. Seismic noise level variation in South Korea. Geosci. J. 13, 183–190.
Sheen, D.-H., Kang, T.-S., Rhie, J., 2018. A local magnitude scale for South Korea. Bull. Seismol. Soc. Am. 108, 2748–2755.
Smith, W.D., 1981. The b-value as an earthquake precursor. Nature 289, 136–139.
Snoke, J.A., 1987. Stable determination of (Brune) stress drop. Bull. Seismol. Soc. Am. 77, 530–538.
Takagishi, M., Hashimoto, T., Horikawa, S., Kusunose, K., ZiQiu, Xue, Hovorka, S.D., 2014. Microseismic monitoring at the large-scale CO_2 injection site, Cranfield, MS, U.S.A. Energy Proc. 63, 4411–4417. https://doi.org/10.1016/j.egypro.2014.11.476.
Tsuboi, S., Abe, K., Takano, K., Yamanaka, Y., 1995. Rapid determination of M_w from broadband P waveforms. Bull. Seismol. Soc. Am. 85, 606–613.
Uchide, T., Imanishi, K., 2018. Underestimation of microearthquake size by the magnitude scale of the Japan Meteorological Agency: influence on earthquake statistics. J. Geophys. Res. Solid Earth 123, 606–620. https://doi.org/10.1002/2017JB014697.
Uhrhammer, R.A., Collins, E.R., 1990. Synthesis of Wood–Anderson seismograms from broadband digital records. Bull. Seismol. Soc. Am. 80, 702–716.
University of Bergen, 2015. NEONOR2 - Kartlegging Av Neotektonik I Nordland. Midlertidige (2 År) Seismometermålinger [NEONOR2 - Mapping of Neotectonics in Nordland. Temporary (2 Years) Seismometer Measurements]. http://nnsn.geo.uib.no/eworkshop/index.php? n=Main.NEONOR-2#tocanchor13.
Westaway, R., Burnside, N.M., 2019. Fault 'corrosion' by fluid injection: potential cause of the November 2017 M_W 5.5 Korean earthquake. Geofluids 2019 (1280721), 23. https://doi.org/10.1155/2019/1280721.
Westaway, R., Younger, P.L., 2014. Quantification of potential macroseismic effects of the induced seismicity that might result from hydraulic fracturing for shale gas exploitation in the UK. Q. J. Eng. Geol. Hydrogeol. 47, 333–350.
Westaway, R., Burnside, N.M., Banks, D., 2020. Hydrochemistry of produced water from the Pohang EGS project site, Korea: implications for water-rock reactions and associated changes to the state of stress accompanying hydraulic fracturing of granite. In: Proceedings, World Geothermal Congress 2020. Reykjavik, Iceland, April 26 - May 2, 2020. Paper 15037, p. 12. https://pangea.stanford.edu/ERE/db/WGC/papers/WGC/2020/15037.pdf.
Woo, J.-U., Kim, M., Sheen, D.-H., Kang, T.-S., Rhie, J., Grigoli, F., Ellsworth, W.L., Giardini, D., 2019. An in-depth seismological analysis revealing a causal link between the 2017 M_W 5.5 Pohang earthquake and EGS project. J. Geophys. Res. Solid Earth 124, 13,060–13,078.
Yeo, I.W., Brown, M.R.M., Ge, S., Lee, K.K., 2020. Causal mechanism of injection-induced earthquakes through the M_w 5.5 Pohang earthquake case study. Nat. Commun. 11 (2614), 12. https://doi.org/10.1038/s41467-020-16408-0.
Yoon, K.-S., Jeon, J.-S., Hong, H.-K., Kim, H.-G., Hakan, A., Park, J.-H., Yoon, W.-S., 2015. Deep drilling experience for Pohang enhanced geothermal project in Korea. In: Proceedings, World Geothermal Congress 2015. Melbourne, Australia, 19–25 April 2015. https://pangea.stanford.edu/ERE/db/WGC/papers/WGC/2015/06034.pdf.
Young, C.J., Chael, E.P., Withers, M.M., Aster, R.C., 1996. A comparison of the high-frequency (& 1 Hz) surface and subsurface noise environment at three sites in the United States. Bull. Seismol. Soc. Am. 86, 1516–1528.